



ALADIN-HIRLAM Newsletter

No. 13, August 23, 2019



Joint 29th ALADIN Wk & HIRLAM ASM 2019

Madrid, 1-5 April 2019

ALADIN Programme, c/o P. Termonia, IRM, Avenue Circulaire 3, 1180 Bruxelles, Belgium
HIRLAM-C Programme, c/o J. Onvlee, KNMI, P.O. Box 201, 3730 AE De Bilt, The Netherlands

CONTENT

Introduction	4
Editorial : Scientific highlights of the Madrid Wk/ASM	5
Events announced for 2019 (and later on)	8
Around the 29h ALADIN Wk & HIRLAM 2019 ASM ... but not only !.....	10
• <u>Benedikt STRAJNAR : Overview of RC LACE data assimilaion activities</u>	<u>13</u>
• <u>David SCHONACH : Ingestion of Clouds into the MetCoOp Nowcasting Model</u>	<u>18</u>
• <u>Florian MEIER, Phillip SCHEFFKNECHT, Christoph WITTMANN, Yong WANG : Nowcasting with AROME – recent challenges and developments in Austria</u>	<u>22</u>
• <u>Ryad el KHATIB : Jumping barriers in AROME</u>	<u>26</u>
• <u>Karl-Ivar IVARSSON: Progress in turbulence, shallow convection and cloud microphysics in MetCoOp</u>	<u>32</u>
• <u>Bent HANSEN SASS : `SLX` verification scheme (Structure of Local eXtremes)</u>	<u>37</u>
• <u>Carlos GEIJO: :Modelling Flow-Dependent Covariances with Gaussian Integrals</u>	<u>41</u>
• <u>Driss BARI and Mohamed AMEKSA: A comparison of datamining tools: visibility estimation from AROME-Morocco outputs by Machine Learning regression</u>	<u>47</u>
• <u>Zahra SAHLAOUI : Case study to assess the precipitation forecast by Moroccan ALADIN configurations</u>	<u>51</u>
• <u>Patricia POTTIER : ALADIN/HIRLAM/LACE Rolling Work Plans : preparation and assessment</u>	<u>54</u>
ALADIN-HIRLAM Newsletters : previous issues	60

Introduction

Welcome to the combined 13th edition Newsletter of the HIRLAM and ALADIN consortia.

The “[29th ALADIN Workshop & HIRLAM All Staff Meeting 2019](#)” took place on 1-5 April 2019 in Madrid (Spain).

This summer 2019 edition is mainly dedicated to this “[29th ALADIN Workshop & HIRLAM All Staff Meeting 2019](#)”.

Therefore, we first like to thank all those that contributed to this Newsletter with their articles.

Please contact authors directly for any needed additional information on their article.

Please be also reminded that a full overview and all presentations (videos and pdf files) can be viewed from the ALADIN website.

Furthermore, an article is dedicated to the new process for the preparation and the assessment of the ALADIN-HIRLAM-LACE Rolling Work Plans.

Last but not least, a summary list of upcoming events, planned for the near future (as from second semester 2019 and after) is available.

We hope you enjoy reading the thirteenth ALADIN-HIRLAM Newsletter. Once again, thanks all authors for their contributions and hand it off first to the PMs for the Edito.

Patricia and Frank

Further consortia information needed?

Please visit the [ALADIN](#) and [HIRLAM](#) websites or contact us.

Edito : Scientific highlights of the Madrid Wk/ASM

Jeanette Onvlee & Piet Termonia

Most of the contributions to this Newsletter represent write-ups of talks and/or posters presented at the Joint 29 ALADIN Workshop/HIRLAM All Staff Meeting 2019. This meeting was held on 1-4 April 2019, in the center of Madrid, on the premises of the Ministry of Ecological Transition.

Hereby are PMs' personal impressions of the scientific highlights of this year's ASM/Workshop.

Data Assimilation

In the first scientific session, on Data Assimilation, one recurrent theme was the continuous struggle to assess new observations and optimize the impact of existing ones. In particular, there was considerable discussion on the issue of quality control and pre-processing of radar observations, especially when radar data from several countries are used simultaneously. The data provided by OPERA are still far from perfect for NWP purposes, and the HOOOF homogenization tool developed by LACE is a good step forward in this respect.

More and more emphasis is given to use the model analysis and forecast system as a nowcasting tool. It is clearly quite challenging still to obtain a consistently good model performance in the nowcasting range, but it was good to see that this issue is being tackled now energetically and from several sides. It was also encouraging to see that more flow-dependent assimilation algorithms (4D-Var, EnVar and LETKF) are approaching operational use.

Finally, our analysis systems are also increasingly in demand for re-analysis applications such as CARRA, and such projects offer an interesting scope for their further improvement.

Dynamics

In the Dynamics session, several presentations clearly showed that there are likely still gains to be made with our present dynamics. However, on the longer-term, adaptations in the model dynamics are clearly required in view of the continued trend towards high resolution and the need to enhance scalability.

The importance of strengthening our efforts on such topics cannot be stressed enough. In this respect, the presentation by Daan Degraauwe, on the performance of two non-spectral solvers using the dynamics dwarf, gave solid and very heartening proof of the excellent prospects that such activities may offer for advancing our NWP systems!

Surface

The Surface session was a relatively short one this year. However, it was very encouraging to see that there is a lot of work ongoing to implement and validate new surface schemes and options into all three CMC's.

In the discussion following the session, the problem was brought up of the (sometimes quite large) local inaccuracies which exist in our global physiographic databases, and the need to supplement these with more detailed information from local GIS data sources. The difficulty here is that we have very limited expertise in how to handle and adapt such data. We should take great care to share such expertise, where available, as effectively as possible!

System

The System session this year was large and covered a wide range of interesting topics, clearly showing the key importance of this work which supports all of us. Several presentations focused on code optimization activities, which, when adding them all up, really help us with the computational challenges of increasing resolution, introducing more advanced physics, larger ensemble sizes, etc. Also, new ways were shown to handle a variety of essential tasks, ranging from a more systematic block testing in the validation of new cycles, to tests of the 903 configuration for LBCs and an alternative setup for building model executables with CMake. Personally, I found the set of this year's system presentations highly enjoyable and quite inspiring!



Essential

Excuses for Not
Writing Documentation

Physics and CMC's

In the Physics session, in addition to the overview presentations on the three CMC's, many presentations touched upon the complex interactions between microphysics, clouds, radiation and aerosols, and the ways in which they are represented in our models. For such studies, the MUSC 1D model environment can be an important tool, but to achieve this, it will be essential to bring MUSC up-to-date with the latest cycle, and to extend it with more special cases for microphysics and cloud aspects.

The talks by Radmila Brozkova and Xiaohua Yang, on respectively the performance of ALARO for high operational horizontal (2.3 km) and vertical (87L) resolution, and the experiences with Harmonie-Arome at sub-km resolutions at DMI, both clearly indicated the advantages of greater spatial detail, the challenges of introducing adequate physiographic data, and the greater insight such studies give us on resolved and unresolved processes in the model.

Verification

In the Verification session, several presentations focused on the redesign and extension of the functionality of the HARP verification system. Later this year, a HARP training will be given to familiarize a wider group of model developers with how to make use of this important tool.

Other presentations showed the continued need for dedicated tools and measures to validate specific model aspects: its performance for local extremes, and the use of simulated imagery especially for nowcasting-related studies.

Ensemble Prediction

The final scientific session was on ensemble prediction. In the past years, we have been spending many efforts on developing and introducing limited area ensemble systems for our three CMC's, with an increasing range of ensemble perturbations. The presentations in this sessions showed that we are now reaching the stage where developers are learning from, and adopting, each other's successful approaches (e.g. different pattern generation techniques, ways of generating physics perturbations, more continuous production etc.)! Something that we can interpret as a clear proof of added value provided by our cooperation, and by the formal and informal exchanges in meetings like these.

Final remark

All in all, a highly varied and interesting meeting. We are already looking forward to its next edition in Ljubljana in 2020!

The PMs

Events announced for 2019 (and later on)

The Newsletters present a static overview (twice a year) with upcoming meetings for the (near) future time frame. For actual updates (year round) please check the [ALADIN](#) / [HIRLAM](#) websites and the [LACE](#) website.

1 ALADIN/HIRLAM related meetings

2019

- [41th EWGLAM and 26 th SRNWP meetings](#), 30 September – 3 October, Bulgaria
- [27th LTM meeting](#), Sofia, 1 October 2019
- [18th PAC meeting](#), Toulouse, 4 November 2019
- [9th Joint HAC/PAC meeting](#), Toulouse, 5 November 2019
- [Regular 24th ALADIN GA](#), Istanbul, 16 December 2019
- 8th HIRLAM-C Council, Istanbul, 16 December 2019
- [5th joint ALADIN GA & HIRLAM Council](#), Istanbul, 17 December 2019

2020

- ALADIN-HIRLAM strategy meeting, early 2020 (tbc)
- [Joint 30th ALADIN Workshop & HIRLAM All Staff Meeting 2020, 30 March - 3 April 2020, Ljubljana, Slovenia](#)
- ALADIN LTM meeting, March 30 or 31 2020, Ljubljana, Slovenia
- HMG-CSSI meeting, April 2-3, 2020, Ljubljana, Slovenia
- Joint ALADIN GA and HIRLAM Council, June 2020 (tbc)

**Joint 30th ALADIN Workshop & HIRLAM ASM 2020
Ljubljana**

host: ARSO Meteo Slovenia

Monday 30 March to Thursday 2 April 14:00

followed by **HMG-CSSI Thursday 2 – Friday 3 April 14:00**

2 ALADIN/HIRLAM Working Weeks / Days

Following topics through working weeks/days will be addressed:

- [Code Training Working Week](#), 9-13 September 2019, Toulouse
- [2019 Joint LACE Data Assimilation and DAsKIT Working Days](#), 18-20 September 2019, Prague
- HARP training, 15-17 October 2019, Copenhagen
- DA working week, 14-18 October 2019, Tenerife
- Lake Workshop, 21-25 October 2019, Toulouse
- EPS working week, 11-15 November 2019, Barcelona
- Surface Working Week, 11-15 November 2019, Maynooth – Ireland

- HIRLAM User Meeting, 19-20 November 2019, Dublin
- System working week, 25-29 November 2019, Oslo [tbc]
- High Resolution and Nowcasting working week, 16-17 December 2019, Canary Isles? [tbc]

3 Regular group video meetings

Regular group video meetings (via google hangouts) are organized for several topics (from both ALADIN and HIRLAM). Outcomes are noted as very valuable. If you like more details how to organize please contact Roger Randriamiampianina, Daniel Santos Munoz or Patrick Samuelsson.

Maria Monteiro (ALADIN DA coordinator) has established regular [specific regular video-conferences with DAsKIT countries](#) (ALADIN DA starter countries).

4 About the past joint events

During the first semester of 2019, besides the big Workshop/ASM (see the links and the articles in this Newsletter), the HMG and the CSSI met on April 5 in Madrid and the HAC and PAC met on May 14 in Norrkoping. The minutes of these meetings have been validated and are on-line (use the links below).

The 7th HIRLAM-C Council was held in Lisbon, June 28, 2019. ALADIN GA members were invited to join the first part of this HIRLAM Council meeting.

On-line information is available through the dedicated ALADIN webpages for past ALADIN/HIRLAM common events such as:

- [joint ALADIN Workshops & HIRLAM All Staff Meetings](#),
- [minutes of the HMG/CSSI meetings](#),
- [minutes of HAC/PAC meetings](#),
- [minutes and presentations : joint ALADIN General Assemblies and HIRLAM Councils](#)

29th ALADIN Wk & HIRLAM 2019

Hosted by AEMET
April 1-4, 2019 in Madrid

In the Agenda below, click on the title of a presentation to get access to the corresponding slides (pdf), or on the title of a poster.

“**article in this Newsletter**” indicates that there is a dedicated article in this newsletter around the presentation/poster.

Click on “**Video**” to get access to the video of the sessions (plenary sessions only).

1 **Agenda** with link to the presentations (videos and pdf files)

- Opening session (**video**)
 - Piet TERMONIA: [ALADIN status overview](#)
 - Jeanette ONVLEE: [HIRLAM highlights of the past year](#)
 - Balazs SZINTAI: [Status of the EUMETNET C-SRNWP project](#)
 - Filip VANA: [ECMWF progress report](#)
- Data Assimilation session (**video 1st part** and **video 2nd part**)
 - Randriamampianina ROGER: [HIRLAM upper-air data assimilation: progress report](#)
 - Benedikt STRAJNAR: [Overview of RC LACE data assimilation activities](#) **article in this Newsletter**
 - Claude FISCHER: [Data assimilation works at MF](#)
 - Joan CAMPINS: [Assimilation of AMDAR humidity observations](#)
 - Schonach DAVID: [Ingestion of Clouds into a Nowcasting Model](#) **article in this Newsletter**
 - Pau ESCRIBA AYERBE: [LETKF with a like-operational HARMONIE-AROME in AEMET](#)
 - Xiaohua YANG: [CARRA reanalysis system: achievement and status](#)
 - Florian MEIER: [Nowcasting with AROME - recent challenges and developments in Austria](#) **article in this Newsletter**
 - Carlos GEIJO: [Towards a NWC application based on HARMONIE-AROME](#)
 - Randriamampianina ROGER: [Impact of observations in HARMONIE-AROME DA during the YOPP SOP1 period](#)
- Dynamics session (**video**)
 - Filip VANA: [Higher order SL advection scheme](#)
 - Petra SMOLIKOVA: [Dynamics in LACE](#)
 - Daan DEGRAUWE: [A robust and scalable non-spectral solver for the ALADIN-NH dynamics](#)
- Surface session (**video**)
 - Patrick SAMUELSSON: [Overview of HIRLAM surface activities](#)
 - Camille BIRMAN: [Snow analysis for NWP at Meteo France and recent developments for land surface analysis](#)
 - Yurii BATRAK: [Recent developments concerning the representation of sea-ice within the ALADIN-HIRLAM NWP system](#)

- Ekaterina KURZENEVA: [Towards Harmonie between CANARI and SURFEX](#)
- Samuel VIANA: [Testing target cy43h surface options in climate mode for assessment & reduction of surface bias: First results](#)
- System sessionsession ([video](#))
 - Daniel SANTOS MUNOZ: [HARMONIE-AROME system status and advancement](#)
 - Ryad EL KHATIB: [Jumping barriers in Arome](#) **article in this Newsletter**
 - Claude FISCHER: [Oops, cycles !](#)
 - Alexandre MARY: [Towards extended validation of new branches and main cycles](#)
 - Martina TUDOR: [Configuration 903 for LBC files](#)
 - Yurii BATRAK: [Experiments with CMake](#)
 - Ole VIGNE: [Single precision experiments with cycle 43](#)
- Physics session ([video 1st part](#) and [video 2nd part](#))
 - Jean-Marcel PIRIOU: [ARPEGE and AROME: recent developments and plans](#)
 - Sander TIJM: [HARMONIE-AROME physics developments](#)
 - Radmila BROZKOVA: [ALARO CMC at high resolution](#)
 - Karl-Ivar IVARSSON: [Progress in turbulence, shallow convection and cloud-microphysics in MetCoOp](#) **article in this Newsletter**
 - Laura RONTU: [About aerosol and cloud particle properties for radiation parametrizations](#)
 - Daniel MARTIN PEREZ: [Use of CAMS Aerosols in Harmonie-Arome](#)
 - Bjorg Jenny ENGDahl: [Results from implementing elements of the Thompson microphysics into HARMONIE-AROME](#)
 - Xiaohua YANG: [DMI experiences with hectometric modelling](#)
 - Eoin WHELAN: [The CY43 MUSC environment](#)
- Verification session([video](#))
 - Bent SASS: [Short summary of HIRLAM-C verification activities](#)
 - Christoph ZINGERLE: [HARP activities and plans](#)
 - Bent SASS: [A new spatial verification scheme for NWP based on analyzing and forecasting local extremes](#) **article in this Newsletter**
 - Andrew SINGLETON: [HARP: more than just a verification tool](#)
 - Angeles HERNANDEZ: [Simulated Satellite Imagery from Harmonie-Arome - Applications](#)
 - Åke JOHANSSON: [Error growth on intra-daily timescales - The importance of the daily cycle in variability](#)
- EPS session ([video 1st part](#) and [video 2nd part](#))
 - Inger-Lise FROGNER: [HarmonEPS developments](#)
 - Martin BELLUS: [LAM-EPS activities in LACE](#)
 - Clemens WASTL: C-LAEF: [Convection permitting Ensemble System of ZAMG](#)
 - Ulf ANDRAE: [Towards continous production and EDA in MetCoOp](#)
 - Alfons CALLADO PALLARES: AEMET-gSREPS: [The Convection-permitting LAM-EPS at Spanish Met Agency](#)
 - Henrik FEDDERSEN: [Experiences with DMI's operational COMEPS ensemble system](#)
 - Geert SMET: [Ensemble forecasting at the RMI of Belgium](#)
 - Endi KERESTURI: [Improving initial condition perturbations for a convection-permitting ensemble prediction system](#)
- Closing session ([video](#)) **edito in this Newsletter**

2 Posters

- Ambar ABDENOUR: [Operational dust aerosol forecasting in Algeria](#)
- Phillip SCHEFFKNECHT: [GSPRO Assimilation Experiments with AROME using Synthetic Data](#)
- Phillip SCHEFFKNECHT: National Poster of the Austrian Weather Service
- Alex DECKMYN: National poster Belgium
- Boryana TSENOVA: NWP in Bulgaria
- Kristian HORVATH: Verification of ALADIN and ECMWF 2m temperature forecasts: towards a joined 7-day forecast
- Iris ODAK PLENKOVIC: An analog approach to wind speed forecasting
- Antonio STANESIC: [The NWP activities in Croatian Meteorological and Hydrological Service](#)
- Mario Hrastinski, Ján Mašek and Radmila Brožková: TKE-based mixing length in TOUCANS
- Alena TROJAKOVA: [NWP activities at CHMI](#)
- Lara QUITIAN HERNANDEZ: Data Assimilation for the study of Subtropical Cyclones
- Patricia POTTIER: [The NWP Systems at Meteo-France](#)
- Balazs SZINTAI: [Biomass and soil moisture simulation and assimilation over Hungary using an offline land surface model with prognostic vegetation](#)
- Mihaly SZUCS: NWP activity at the Hungarian Meteorological Service
- Colm CLANCY: [Dynamics Research at Met Eireann](#)
- Ronan DARCY: [Irish Regional Ensemble Prediction System \(IREPS\)](#)
- Emily GLEESON: [Radiation in HARMONIE-AROME](#)
- Alan HALLY: IREPS: The Irish Regional Ensemble Prediction System
- Roohollah AZAD: 3DVAR Assimilation of Aeolus HLOS wind in Harmonie-Arome
- Randriamampianina ROGER: RadPrO project: using crowd-sourced observations to improve weather condition analyses and forecasts
- Ole VIGNES: [MetCoOp status and plans](#)
- Bogdan BOCHENEK: [Poland - national poster](#)
- Maria MONTEIRO: [2019 NWP activities at IPMA](#)
- Alexandra CRACIUN: [ALADIN activities in Romania](#)
- Maria DERKOVA: [ALADIN related activities @SHMU](#)
- Martin DIAN: [INVESTIGATING SURFEX IN ALARO-1](#)
- Michal NESTIAK: Our steps in DA
- Jure CEDILNIK: ALADIN in Slovenia 2019
- Javier CALVO: [AEMET NWP activities](#)
- Carlos GEIJO: Modelling Flow-dependent Covariances with Gaussian Integrals **article in this Newsletter**
- Esbjorn OLSSON: Harmonie-Arome High Resolution forecasts for Alpine World Ski Championships
- Khalfauoui Wafa: NWP Activities in Tunisia
- Alper GUSER: Aladin Related Activities in Turkey

3 Working groups, side-meetings, LTM meeting, HMG/CSSI meeting, ...

More information on the 29th Wk&ASM 2019 ([agenda](#) and [participants](#), photos) and the side events (WG discussions, LTM meeting, HMG/CSSI meeting) are available on [the dedicated page on the ALADIN website](#).

Overview of RC LACE data assimilation activities

compiled by Benedikt Strajnar

1 Introduction

This contribution is a summary of recent DA assimilation activities within the RC LACE data assimilation teams, and summarizes work of many contributors from the involved member countries. It includes an overview of operational status, algorithmic developments for upper-air and surface, and development related to preprocessing of radar observations.

2 Operational status

Most RC LACE countries currently run 3-hourly 3D-Var analysis and surface analysis with CANARI, cy40. In the Czech Republic, their operational BlendVar system version is cy43 and the horizontal resolution was upgraded from 4.7 to 2.3 km. Recently, the model version was also upgraded to cy43t2 in Slovenia. Some countries improved their use of observations.

Table 1: Data assimilation - operational status in RC LACE countries with 2019 improvements to model versions marked in orange.

Country	AT	AT	CR	CZ	HU	HU	SK	SI	RO
<i>Physical package</i>	Phys.	AROME	ALARO	ALARO	ALARO	AROME	ALARO	ALARO	ALARO (preop.)
<i>Resolution</i>	4.8L60	2.5L90	4L73	2.3L87	8L49	2.5L60	4.5L63	4.4L87	6.5L60
<i>Cycle</i>	40t1	40t1	38t1	43t2_bf8	38t1_bf3	38t1_bf3	40t1	43t2	40t1
<i>Coupling</i>	IFS 3h (lag.)	IFS 1h (lag.)	IFS 3h (lag.)	ARP 3h	IFS 3h (lag.)	IFS 1h (lag.)	ARP 3h	IFS 1h/3h (lag.)	ARP 3h
<i>Assim. algorithm</i>	OI + dyn. adapt	OI_main MESCAN + 3DVar	OI + 3DVar	OI + BlendVar	OI + 3D-Var	OI_main + 3D-Var	OI + DF Blending	OI + 3D-Var	OI + 3D-Var
<i>Cycling</i>	6h	3h	6h	6h	6h	3h	6h	3h	6h
<i>B-matrix</i>	-	Downscaled LAEF	NMC	Downscaled AEARP	ALARO EDA	AROME EDA	-	Downsc. ECMWF	Downsc. AEARP
<i>Initialization</i>	DFI	No (SCC)	No (SCC)	IDFI in prod., SCC			No	No (SCC)	No (SCC)
<i>Additional</i>	Additional snow melt	Snowgrid +SAT snow init.	Mode-S MRAR	Mode-S MRAR Mode-S EHS		GNSS ZTD		HRW, IASI, ASCAT, Mode-S EHS	

3 Algorithmic developments

Hourly updated assimilation systems

The hourly updated systems were mainly studied in Austria and in Hungary with their AROME RUC. Figure 1 shows a result from Hungary, where a hourly 3D-Var was combined with surface optional interpolation at various time resolution (1 h, 3 h, 6 h). Results indicate that combining the 3- and 6-hourly OI in the hourly system improved 2 m temperature and relative humidity and well as precipitation scores compared to 1-hourly surface data assimilation. It was shown that a somewhat smaller amount of surface observations for each hourly analysis is not the main contributing factor to this degradation. It is more likely to be related to biases introduced to soil during the OI_MAIN analysis step.

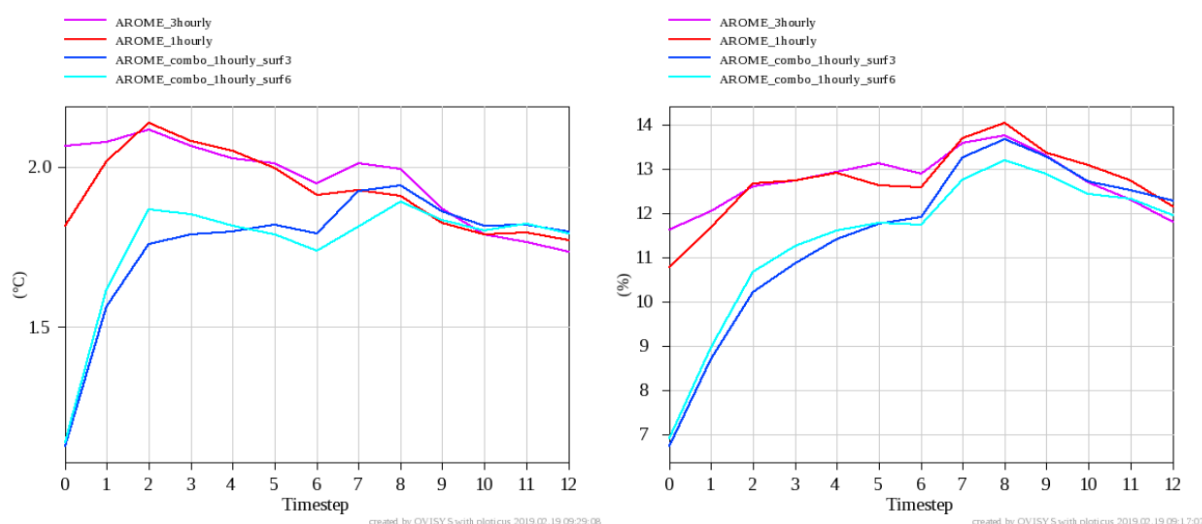


Figure 1: RMSE of 2 m temperature (left) and relative humidity (right) in time (hours) for different combinations of hourly 3D-Var and 1, 3 and 6-hourly surface analysis.

Properties of background errors

Background errors were further studied in Croatia by comparing three different B-matrix sampling approaches and their influence on forecast. The study involved B-matrices derived using standard National Meteorological Center (NMC) and two ensemble data assimilation (EDA) methods, one with unperturbed LBCs (ENS) and one with perturbed LBCs (ENSLBC). Diagnostic comparison showed that ensemble techniques shifts correlations towards small scales. This is most pronounced for ensemble with unperturbed LBCs. The use of the new ENSLBC based B-matrix reduces spin up in first hours of forecast. The verification shows modest improvement for experiment with new ENSLBC based B-matrix compared to the NMC-based one. In the Czech republic, a set of ENS-based B-matrices at different resolution and season was inter-compared. A large sensitivity of high-level humidity was observed and a REDNMC tuning was needed in their new 2.3 km system to improve scores.

Study of Var-BC performance in LAM

The continuation of work on Var-BC for satellite radiances in LAM was focussed on tuning the adaptivity, either statically or dynamically (where the adaptivity changes with number of observations). Two approaches were considered: adjusting the adaptivity (NBG parameter) and implementation of dynamic adaptivity (after Cameron and Bell, 2016). Extensive testing showed that the methods involving Var-BC in LAM methods outperform the use of coefficients from ARPEGE providing the better quality of the first-guess in the 3-hour assimilation cycle with the largest normalized impact of 2 – 3% for temperature and wind components in middle troposphere (Fig. 2).

Although the differences are rather small, it is evident that in the LAM, the locally cycled experiments all outperform the global ones.

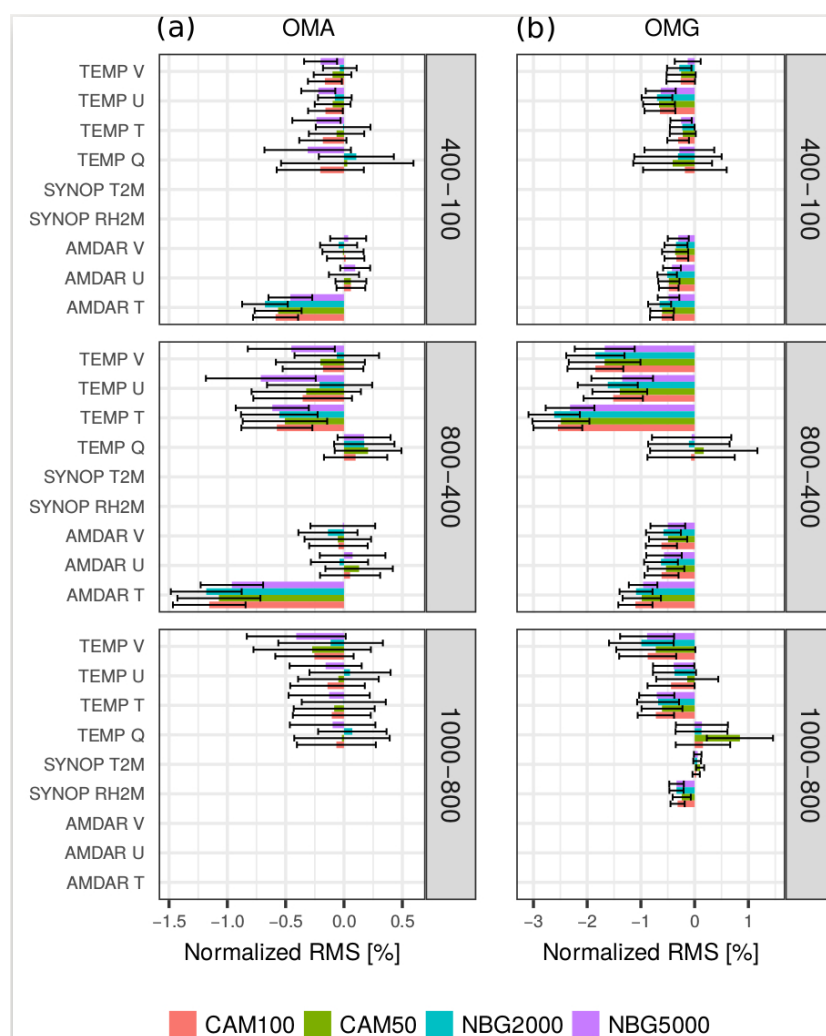


Figure 2: The normalized RMS of OMA (a) and OMG (b) residuals evaluated for different VarBC-LAM configurations (CAM stands from Cameron and Bell (2016), NBG to modified adaptivity setting) with respect to conventional observations from 01 Dec 2015 to 31 Jan 2016. The VarBC-global method is used as a reference experiment. Error bars represent 95% significance level.

Advances in surface data assimilation

The efforts in surface data assimilation were devoted into implementation of the ensemble Kalman filter (EKF). In Austria, the control variable set was extended with soil temperature, water and ice at eight levels in the ground. A local observation error maps were created by comparison between remote-sensed and modeled data. It was found that assimilation of SCATSAR_SWI observations (green color in Fig. 3) significantly improves temperature RMS and bias at 2 m in the short-range AROME forecast. A paper on this is submitted for publication (Schneider and Bauer-Marschallinger, 2019). EKF is also being evaluated in Slovakia where a novel method to compute the H-derivatives was developed. INCA T2 analysis was introduced as grided observation source to deduce the soil increments (not shown).

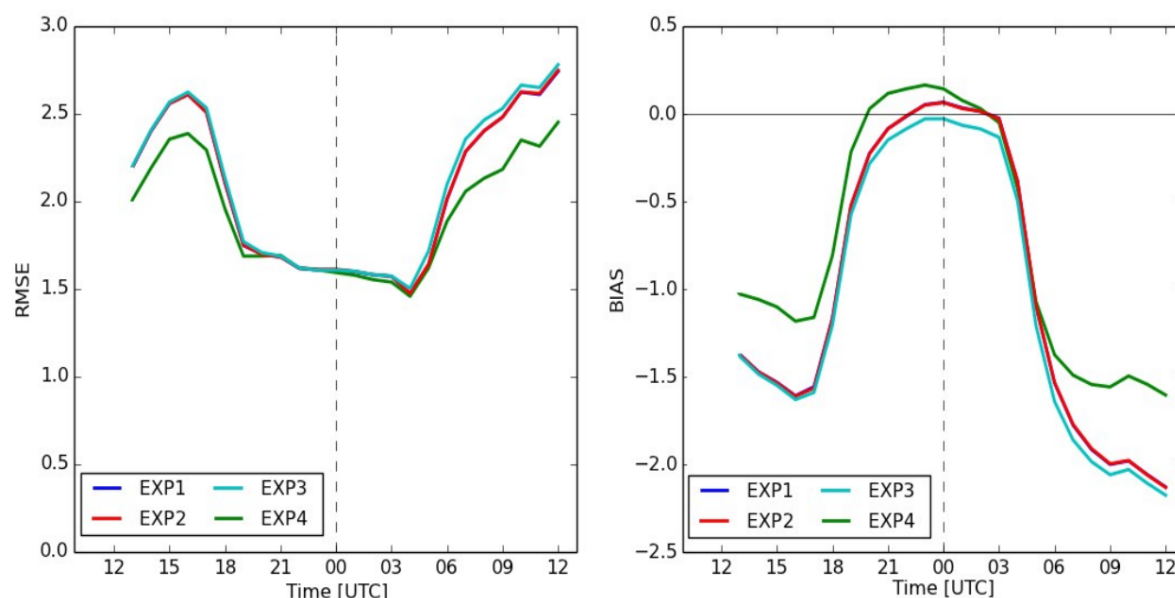


Figure 3: Assimilation of SCATSAR-SWI in Austria: RMSE (left) and bias (right) for T2M forecasts from 20160501-20160629, averaged for all SYNOP stations in Austria located below 300 m. EXP1 is the reference run, EXP2 and EXP3 are experiments with assimilation of superficial soil moisture, EXP4 is with assimilation of all available soil moisture data (down to ~60 cm in the ground).

4 Observation developments

Towards assimilation of OPERA radar

Several countries started tests with the OPERA/OIFS volume radar data, and it was found that despite it comes in a common data format (ODIM), the data structure is not always the same and metadata is sometimes still incomplete. A Python-based tool called HOOFF was therefore developed with the following functionality: splitting the data by time into individual measurements, reorganizing it in a way that there is one data set for one elevation, providing the same quality flags, filling in the metadata in a flexible way and retaining only what is requested for assimilation. The tool is namelist-driven and the namelist defines what data to process, which radar moments, and the structure and attributes contained in the output file with default values. It is also possible to predefine or change value for specific radar site if an extra block is added. There is also a companion meta-data browser which enables an easy way to check values of a given attribute over the whole dataset. The tool is available for testing in a wider community (Smerkol, 2019).

The assimilation experiments were so far mostly performed only in Austria. Their evaluation reported challenges related to the quality of first guess for radar data assimilation. Figure 4 shows the radar assimilation performance on a case with severe convection around Vienna, Austria, in comparison to INCA precipitation analysis. The convection in the center of domain is clearly missing in the AROME forecast (bottom left) despite that the strong echos existed in the radar measurement (seen through INCA analysis) – this was due to absence of convection over the area in the first guess for assimilation. The situation can be somewhat improved if saturated profiles are applied above a certain reflectivity threshold.

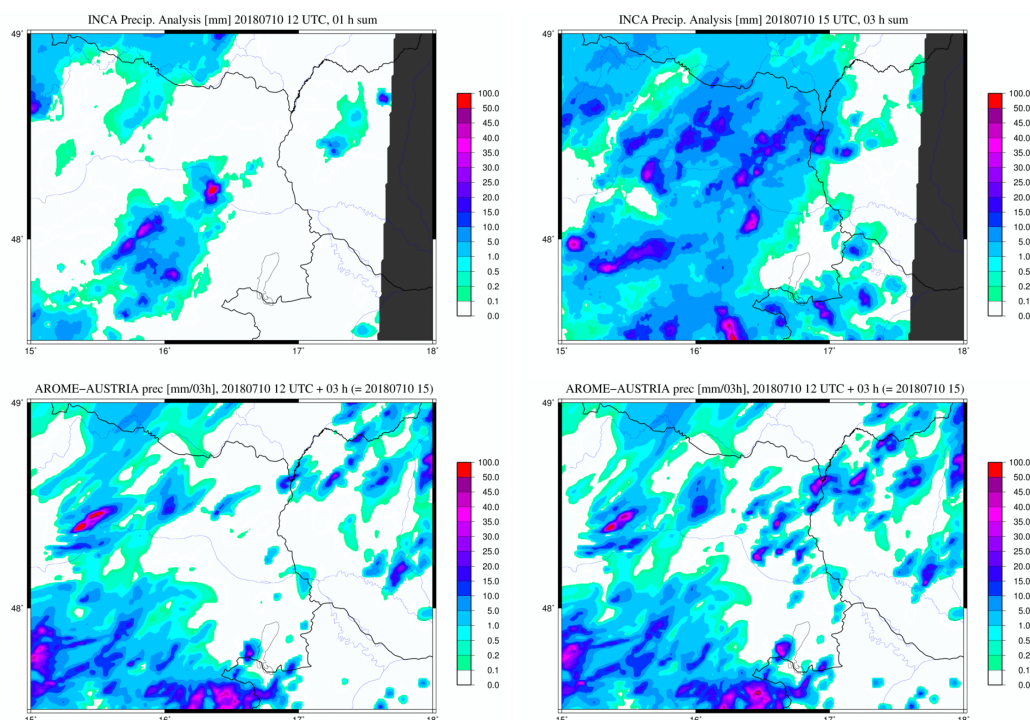


Figure 4: Case study of flash flood in Vienna (center of the map) on 10 July 2018: INCA precipitation analysis before model init time (top left), INCA accumulation during first 3 hours of integration (top right), AROME-RUC1.2+RADAR (bottom left) and the same setup using saturated profiles if threshold on DBZ exceeded (bottom right).

5 Summary and outlook

The activities of RC LACE assimilation group are focused on operational application of data assimilation of high-resolution LAMs, which includes refinements of existing upper-air assimilation algorithms, gradual introduction of improved surface assimilation schemes (EKF) and additions of as many different observations as possible. In this contribution the work on volume radar measurements provided by OPERA was described: the dataset with a large potential but also challenges due to significant heterogeneity in the radar systems across the central Europe. Other high-resolution observations networks such as Mode-S aircraft observations, GNSS-derived data and other humidity-related observations were not described here but are continuously evolved within RC LACE.

6 References

- Cameron, J. and Bell, W.: The testing and planned implementation of variational bias correction (VarBC) at the Met Office, Met Office, Exeter, UK, 2016. https://cimss.ssec.wisc.edu/itwg/itsc/itsc20/papers/11_01_cameron_paper.pdf
- Schneider, S. and Bauer-Marschallinger, B.: Assimilation of SCATSAR Soil Wetness Index in SURFEX 8.0 to improve weather forecasts, Geosci. Model Dev. Discuss., <https://doi.org/10.5194/gmd-2018-273>, 2019.
- Smerkol, P.: HOOF software and manual ,RC LACE forum, 2019. <http://www.rclace.eu/forum/viewtopic.php?f=37&t=582>

Ingestion of Clouds into the MetCoOp Nowcasting Model

David Schönach, Erik Gregow

1 Introduction

Correct cloud-initialization is a critical procedure in Numerical Weather Modelling as clouds govern for example over long- and shortwave radiation processes and therefore affect many variables directly (Jimenez, 2016). Our work of ingesting clouds into the MetCoOp Nowcasting Model (MNWC, currently running on harmonie c40h-1.2 in pre-operational mode) concentrates on using satellite and ground-based observations to find the correct cloud-placement. We concentrate on using the heights of cloud top and cloud base in our ingestion process. We also investigate a method of cloud-layering inside a cloud, where we use the model tendencies of relative humidity.

2 Assessment

2.1 Cloud top

The height of the Cloud top is assigned by using the measurements of brightness temperature from the satellite and comparing it to the model's vertical temperature profile. The Cloud top is therefore well-measured and data from geostationary satellites cover the whole domain.

2.2 Cloud base

Finding the correct cloud base is more difficult. We combined a firstguess field of cloud bases and ground-based measurements of cloud bases.

The firstguess field of cloud bases is a "spreaded" field, which are a postprocessed variable in MetCoOp-Ensemble-Prediction-System (MEPS). We used a 2h forecast of the control MEPS member (Figure 1 a). The term "spreaded" refers to the incrementally spreading of the cloud bases in horizontal space (illustrated in Figure 1) to insure that we also capture for example newly formed/growing convective clouds, which are not well positioned (or displaced) in the firstguess.

The spreaded field of cloud bases (Figure 1 d) is thereafter merged with the SYNOP and METAR measurements of cloud bases. The optimal interpolation was used for that purpose and the software used was GridPP (<https://github.com/metno/gridpp>). GridPP can use gridded data in netcdf format and stationwise data (e.g. observations) in netcdf or ascii format. Unlike Canari GridPP is open source and it is maintained by colleagues of METNorway. GridPP is mainly used for postprocessing.

Figure 2 shows the final field of cloud bases, our "analysis" of cloud bases after spreading the firstguess field, interpolating with the observations and applying the true satellite cloud mask.

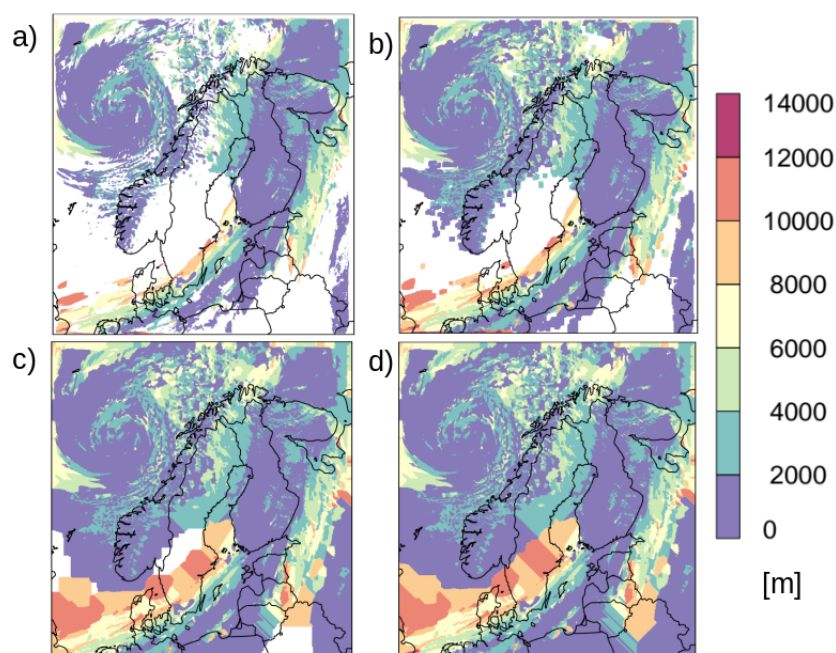


Figure 1: Creation of First-Guess field of cloud bases. a) is 2h MEPS forecast of the control member. b)-d) shows the method of spreading the cloud bases values in horizontal space.

2.3 Results

Observations were verified out-of-sample against the forecast fields of cloud bases (Harmonie-A., which stands for Harmonie-Arome) and against the result of the whole procedure (“Analysis” Figure 3). Figure 4 shows that the method significantly improves the cloud bases in terms of Root-Mean-Square-Error (RMSE) and correlation coefficient.

2.4 Using cloud top and cloud base in MNWC

Cloud top and cloud base cannot be inserted as direct model inputs into the MNWC system. We use a 3d-approach of modifying the temperature and moisture vertical profiles with respect to this new information (Figure 4). At new cloud tops and cloud bases we add moisture up to saturation. Above cloud tops and below cloud bases we remove moisture down to a value of moisture where clouds are not expected (Quaas, 2012). This work is ongoing.

3 Conclusion

In principal, combining cloud-measurements from satellites and from SYNOP and METAR observations with the described approach showed to give better fields of cloudbases.

We currently work on implementing this new cloud information into the preoperational version of MNWC. In addition to the method of only modifying the moisture and temperature profiles we also consider modifying cloud nuclei.

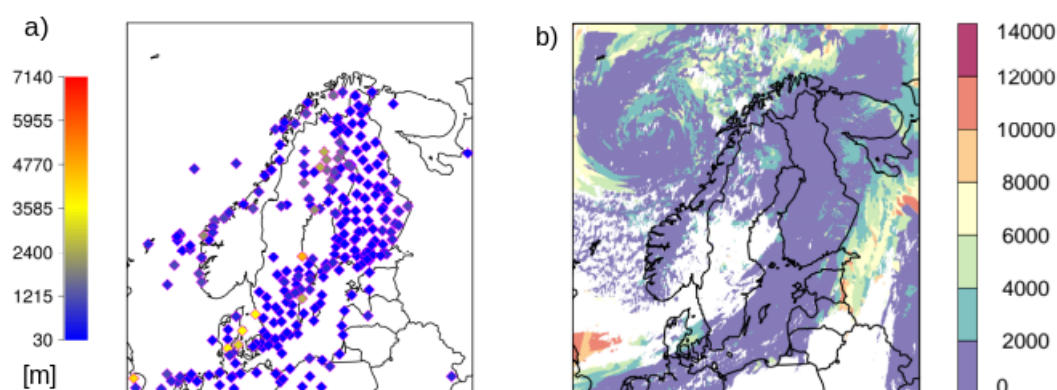


Figure 2: a) Station locations of SYNOP and METAR observations of cloud bases. b) Our "Analysis" = field of cloud bases after interpolation of spreaded firstguess field (Fig.1d) with SYNOP and METAR observations (a).

Further the use of polar satellites would add better quality especially in higher latitudes than the geostationary satellites. But their coverage is bad and sometimes only small parts of the MetCoOp domain is covered.

4 Acknowledgement

We acknowledge financial support by the Strategic Research Council of Academy of Finland (decision no. 292854) and by Finnish civil aviation funds.

5 References

- Jimenez, Pedro A., et al. "WRF-Solar: Description and clear-sky assessment of an augmented NWP model for solar power prediction." *Bulletin of the American Meteorological Society* 97.7 (2016): 1249-1264.
- Quaas, Johannes. "Evaluating the "critical relative humidity" as a measure of subgrid-scale variability of humidity in general circulation model cloud cover parameterizations using satellite data." *Journal of Geophysical Research: Atmospheres* 117.D9 (2012).

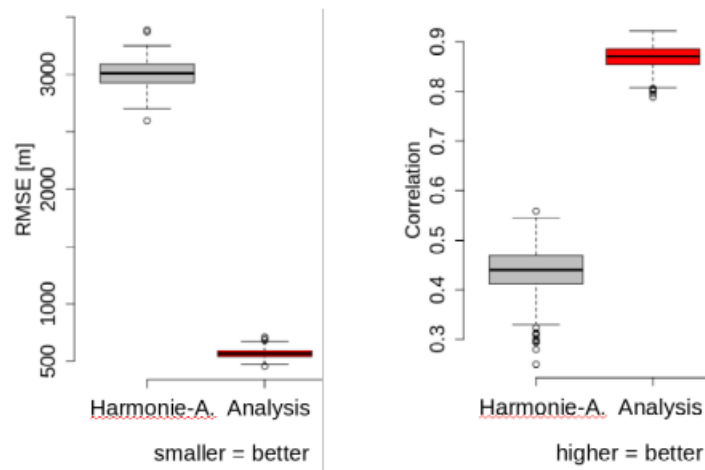


Figure 3: Results of out-of-sample verification of original field of cloud bases from MEPS and "Analysis" field of cloud bases against the SYNOP and METAR observations. Left is the RMSE and right the correlation coefficient.

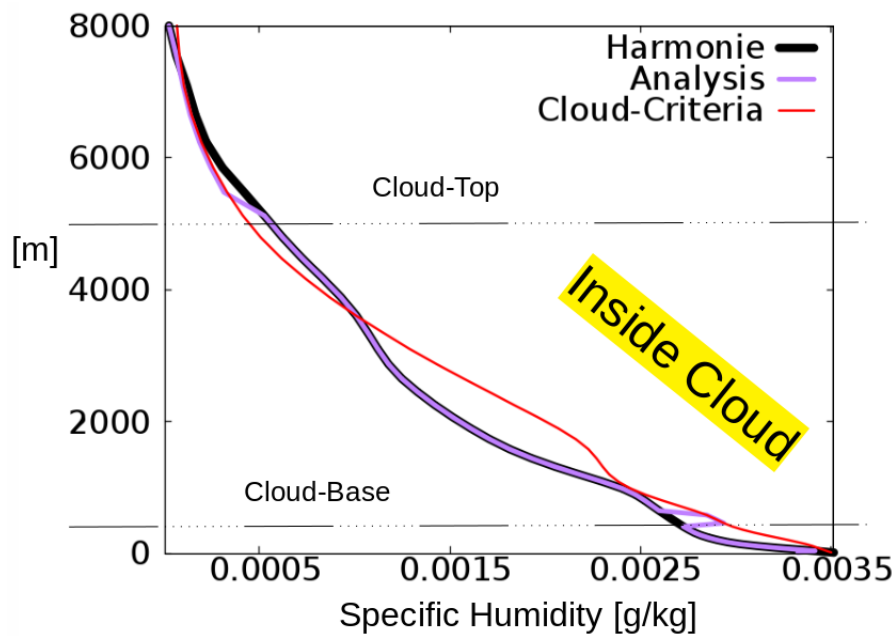


Figure 4: Illustration how the 3d-approach in the vertical dimension should look like. For modifying moisture and one grid-point.

Nowcasting with AROME – recent challenges and developments in Austria

Florian Meier, Phillip Scheffknecht, Christoph Wittmann, Yong Wang

Introduction

For several years, an hourly AROME based nowcasting system on a 1.2 km x 90 L grid has been developed at ZAMG in Austria. It will become operational by the end of 2019. Similar systems are currently tested or already in operations in several countries (for example France (Auger et al. 2015), Denmark, Norway, Hungary, United Kingdom, USA). In addition to these other examples, the Austrian system includes latent heat nudging of classical nowcasting analyses and forecasts up to +35min (Meier 2015), FDDA nudging of automatic weather stations up to +30min and saturation of radar profiles if observed precipitation is not present in the model (proposal of E. Wattrelot 2015; personal communication). In the most recent version, variational quality control (VARQC) of Doppler wind observations is switched on to reduce the negative impact of incomplete de-aliasing. Further, it is a cycled system with hourly LBCs from AROME-Aut 2.5km. The B-Matrix is derived from a 2.5km C-LAEF ensemble driven 1.2 km EDA (Berre 2000). The system improves the 10 m wind and gust forecasts for the whole forecast range compared to AROME-Aut 2.5 km and precipitation forecasts up to +6h.

Table 1: main settings of the AROME-RUC nowcasting

Model version	AROME cy40t1 export + local modifications
Grid space / vertical levels	1.2km / 90
Area	Austria and surrounding 900x576GP
Initial conditions	Hourly 3D-Var+LHN+FDDA-Nudging+IAU
Boundaries	Hourly AROME-Aut 2.5km L90
Soil initialisation	Hourly CANARI-OIMAIN; at 23 UTC PREP
Maximum lead time / Timestep	12h / 30s
cycling interval	1 hourly; at 23 UTC the first guess is taken from AROME-Aut 2.5km
Observation window	-90min/ +30min

1 Spin-Up behaviour and cycling strategy

Comparison of an hourly and a two-hourly-cycled system showed much larger precipitation and wind biases in the hourly system. Therefore, the spin-up behaviour at selected grid points was investigated with ECHKEVO diagnostics. This showed, that spin up undulations last longer than one hour and that they are not related to the implemented nudging. Spin-up artefacts are especially intense when the first guess is downscaled from driving model AROME-Aut 2.5 km (open loop with change in resolution). On the other hand, a sufficiently long incremental analysis update window allows to filter the undulations. Therefore, a new system with a 50 min incremental analysis update (IAU, Merlet et al. 2017) window was tested, showing comparable performance to the two hourly cycle. This model version is started one hour before the analysis time and pushed towards the current 3D-Var analysis by the IAU over 45 minutes. The current run is then started based on this rerun and pushed towards the analysis for five more minutes, such that there is almost no interference between nudging and IAU, but

the spin-up artefacts are satisfactorily filtered out. A long IAU period seems to significantly affect the hydrometeors. Therefore, they are blended from the freely running first guess before the integration.

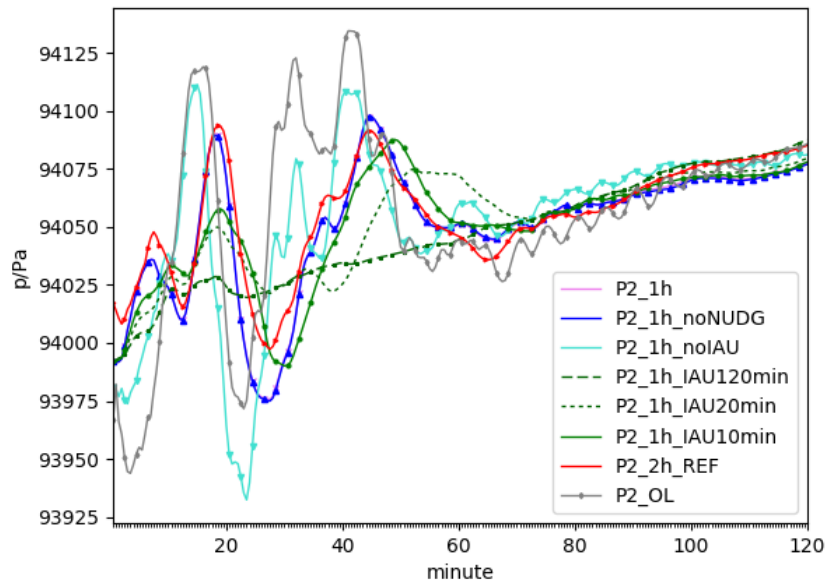


Figure 1: Spin-Up diagnostics for a selected grid point. Pressure as function of lead time in minutes. Different experiments including different lengths of IAU windows (pink reference is IAU 5min) in hourly cycle as well as 2h cycle (red), open loop, where first guess is downscaled from AROME-Aut 2.5km (OL, grey) and experiments, where nudging is switched off (blue) with no significant difference to the pink reference.

2 Saturation of radar profiles

The 3D-Var assimilation of radar reflectivity follows the 3D+1D approach of Wattrelot and Caumont. This approach struggles if the first guess differs strongly from the observation, e.g. radar observed precipitation with the model not showing any corresponding signal in the same area. In that case, a saturation of the pseudo humidity observation profile is applied, if the observed reflectivity exceeds a certain threshold (50dBz, 7dBz, 12dBz). While this modification in `inv_refl1dstat.F90` was beneficial in singular cases, a positive precipitation bias was found in a longer test period. Therefore, the thresholds were re-tuned to 55dBz (set humidity pseudo obs to minimum of 100% in any case), 15dBz (set humidity obs to minimum of 97% (95% in old setting) if simulated reflectivity is below 0.01 and 25dBz (set humidity obs to minimum of 100% if simulated reflectivity is below 0.01).

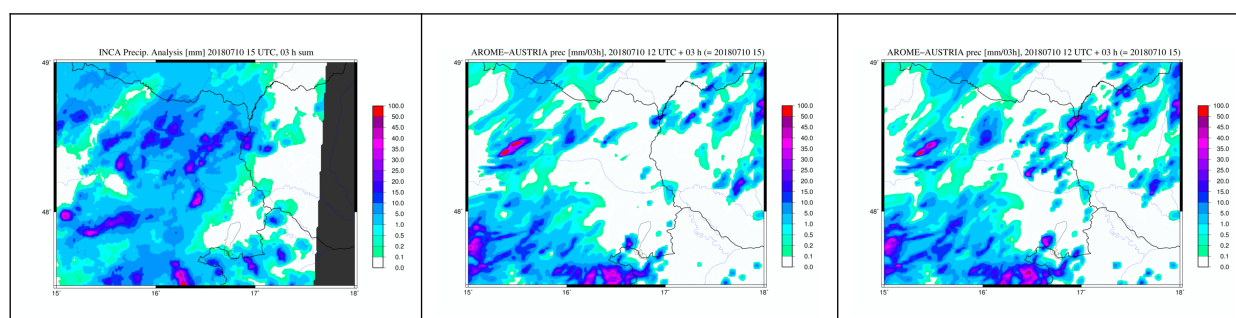


Figure 2: Example of useful effects of saturated radar profiles for the precipitation forecast on 10th July 2018: A flash flood was observed and is visible in the INCA precipitation analysis (left) in the Vienna river catchment, requiring the rescue of several workers. This is not forecast at all, using AROME and 3D-Var radar assimilation (middle), but simulated when the saturation of profiles, as described in the text, was used, albeit with some displacement remaining (right).

3 VARQC

Based on first tests in HIRLAM 4D-Var working week in Norrköping in 2010, VARQC (Andersson and Järvinen 1999, Holm 2014) is switched on and tuned for Doppler wind observations. The observation impact analysis had shown a spurious impact of Doppler wind observations in the AROME-RUC, which is likely related to incomplete de-aliasing of Doppler winds. VARQC provides the opportunity to reduce the weight of suspicious observations with large first guess departures without rejecting all Doppler winds of such a radar station. However, a better de-aliasing would be preferable. It is found that Doppler winds show an error statistic suitable for VARQC in the system (Fig. 3). The Huber norm with the following settings is chosen:

Table 2: settings of VARQC for Doppler winds

LVARQCG=TRUE
LHUBERMINQCG=TRUE
LHUBERMINQC(44,13)=TRUE
LHUBERBGQC(44,13)=TRUE
RHUBERBGQC(44,13,13,1:3,1)=8
RHUBERBGQC(44,13,13,1:3,2)=15
RHUBERBGQC(44,13,13,1:3,3)=26
RHUBERRIGHT(44,13,13,1:3)=8
RHUBERLEFT(44,13,13,1:3)=8

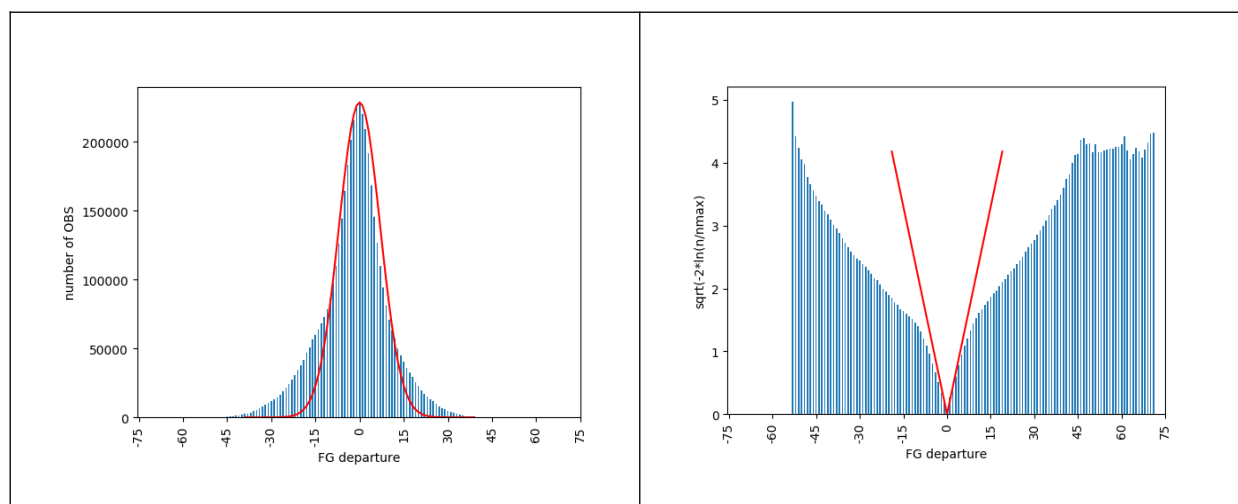


Figure 3: Raw (left) and rescaled (right) first guess departures of Doppler wind observations from AROME-RUC (one week of data from July 2016). At around $\pm 8m s^{-1}$, the distribution deviates from a linear (Gaussian like) behaviour defining the HUBER parameters.

A significant reduction of the cost function J_0 of Doppler winds by almost 50% can be achieved by the new setting and a slight improvement in the precipitation forecast is also found.

4 Outlook

Since April 2019, the system, including hourly cycling, saturation of radar profiles, and VARQC of Doppler winds, is running in real time at ZAMG. Future plans for development will focus on applications and driving the classical nowcasting system INCA with AROME-RUC. Furthermore, the assimilation of private weather stations, wind profilers and an improvement of de-aliasing procedures is envisaged.

5 References

- E. Andersson and H. Järvinen, 1999: Variational quality control. *Q. J. R. Meteor. Soc.*, 125, 691-722.
- L. Auger, O. Dupont, S. Hagelin, P. Brousseau and P. Brovelli, 2015: AROME-NWC: a new nowcasting tool based on an operational mesoscale forecasting system. *Q. J. R. Meteor. Soc.*, 141(690), 1603–1611.
- L. Berre, 2000: Estimation of Synoptic and Mesoscale Forecast Error Covariances in a Limited-Area Model. *Mon. Wea. Rev.*, 128, 644-667.
- E. Holm, 2014: Variational Quality Control. Lecture at data assimilation training course at ECMWF, Reading, UK.
- F. Meier 2015: Radar assimilation and latent heat nudging in AROME Nowcasting/AROME-PI. RC-LACE stay report, Toulouse, available at www.rclace.eu/File/Data_Assimilation/2015/reportLACEstaymeierautumn2015.pdf
- N. Merlet, P. Cau, C. Jauffret, K. Maynard, I. Sanchez and P. Brousseau, 2017: AROME-NWC Overview, Results, Evolution and Perspectives. Newsletter 22, p40-42, of The European forecaster WGCEF available at: [http://www.euroforecaster.org/gpeasy/gpEasy_CMS/Newsletter22_\(2017\)](http://www.euroforecaster.org/gpeasy/gpEasy_CMS/Newsletter22_(2017)).
- E. Wattrelot, O. Caumont and J.-F. Mahfouf, 2014: Operational Implementation of the 1D+3D-Var Assimilation Method of Radar Reflectivity Data in the AROME Model. *Mon. Wea. Rev.*, 142, 1852-1873.

Jumping barriers in AROME

Ryad El Khatib

1 Introduction

The code of AROME is subject to various technical limitations, penalizing its development or its computational performance. Four of them are discussed in this paper :

- the bounds violations at runtime
- the sensitivity to memory bandwidth in the software
- the problem of the extension zone for scalability
- the load imbalance cause by the meteorology nature in the distributed geometry

2 The bounds violations at runtime

2.1 Origins of the arrays bounds violations issue

Models fail at runtime when the whole code is compiled with arrays bounds checking option because of several "assumed" violations.

These violations are "assumed" because the code has been written in such a way that it should remain flexible for scientific researches and developments, and designed at the time the Fortran norm was Fortran 77.

Here is a typical example :

```
REAL (KIND=JPRB) , INTENT (IN) :: PGMVT1 (NPROMA, NFLEVG, NDIM)  
CALL GPINISLB ( . . . , PGMVT1 ( 1, 1, MNHX ) , . . . )
```

Inside the subroutine GPINISLB the variable PGMV(:, :,MNHX) will be used only if the model is non-hydrostatic. Consequently the address MNHX will be uninitialized (or initialized to a value out of the bounds of the array PGMV) if the model is hydrostatic. This will be harmless ... as long as PGMV(:, :,MNHX) is not used by mistake. Therefore the check against arrays bounds violation would be helpful to avoid such bugs.

Unfortunately, once we have assumed that we would not do such mistakes in a given subroutine, we have to assume that the whole subroutine concerned cannot be compiled with arrays bounds checking option, and that may hide other bugs.

As a partial workaround, we may set the default address to the value of the variable NUNDEFD which is in namelist. Its default value is a number huge enough to cause bounds violations, but if set to 1, then the potential bounds violations will be silent ... to the risk that the model returns wrong results !

With the Fortran 90, a possible solution was to use optional arguments. That solution has been used here and there, but it has its limits : the code becomes very difficult again to maintain with increasing number of options, leading to combinations of optional arguments.

2.2 Solution to the arrays bounds violations

A final solution is being developed, and might be implemented in the common cycle 47.

The general idea is to consider that we don't want to determine by ourselves the memory address of a field (or a group of fields) but, as users, we request a field from a fields database and we expect the system to return its memory address to us.

Following this idea we can take advantage of Fortran pointers, not used as allocatable entities but only as true pointers.

The pointers will be computed by a generic function, given the array of origin and the estimated address inside. Let's consider its application to the first example above :

```
USE SC2PRG_MOD, ONLY : SC2PRG ! Generic function
REAL(KIND=JPRB), INTENT(IN) :: PGMVT1(NPROMA,NFLEVG,NDIM)
REAL(KIND=JPRB), POINTER :: ZNHXT1(:, :) ! User pointer declaration
CALL SC2PRG(MNHX,PGMVT1,ZNHXT1) ! Pointer initialization
CALL GPINISLB(..., ZNHXT1,...) ! Pointer instead of the direct addressing
```

The generic function will check the size of the array and the given address against the array bounds. If the given address is valid (within the array bounds) and the size of the array is not zero, the pointer is initialized to the proper address. Otherwise the pointer is initialized to null. At runtime there won't be any bounds violation but if a pointer with null address is used, then the model will abort on a segmentation violation signal.

2.3 Implementation

This solution has been implemented on top of cycle 46t1_r1.03, and tested successfully on a toy IFS application, and on ARPEGE and AROME at high resolution. Other tests on TL and AD models at low resolution have been tested successfully, too. A test of IFS 4Dvar is expected from ECMWF.

The modifications of code have a neutral impact on the computational performance, and had a null impact on the scientific results.

36 subroutines are directly concerned by the modifications for fixing bounds violation, though not all of them had needed the generic pointer function. For safety, most of them have been transformed thanks to a basic script.

From the moment this solution is implemented in the code, executions of the model with the code compiled integrally with arrays bounds checking should be regularly performed ; and no arrays bounds violations should be tolerated anymore.

3 The sensitivity to memory bandwidth in the software

AROME is highly sensitive to the amount of memory accesses, which is something different from the amount of memory used.

Data accessed from the memory (well-known as "Random Access Memory") by the processor transit by the memory cache, which is very fast but small memory banks, transported by narrow memory buses. Too much or too frequent accesses can cause the buses to be overloaded, or the memory cache to be overloaded, and this would slow down the computation (the bottleneck being the memory buses, not the CPU).

Such sensitivity to that "memory bandwidth" is caused by excessive arrays initializations or copies, and, to some extent, by the use of array syntax in calculation (reducing the opportunity of re-using data in memory cache).

A typical example of subroutine making excessive use of memory bandwidth is `apl_arome`, the interface of

the model to the physical parameterizations of AROME. This routine has been substantially re-written in order to remove initializations or copies wherever possible. These modifications made the subroutine almost 2 times faster.

The following example is a tip recommended to be used to remove safely useless arrays initializations : in the code below the initialization of the array X is useless ; while the initialization of Y is needed :

```
X(:)=0.
Y(:)=0.
DO J=1,N
  X(J)=F(J)
  Y(J)=Y(J)+X(J)
ENDDO
```

The suggestion is to code a conditional initialization, for testing purpose :

```
! INIT0 = 0 : initialization to HUGE
! INIT0 = 1 : initialization to a realistic value
! INIT0 =-1 : No initialization at all
INIT0=1
IF (INIT0 == 0) THEN
  ZVALUE=HUGE(1.)
ELSE
  ZVALUE=0.
ENDIF
IF (INIT0 >= 0) THEN
  X(:)=ZVALUE
  Y(:)=ZVALUE
ENDIF
DO J=1,N
  X(J)=F(J)
  Y(J)=Y(J)+X(J)
ENDDO
```

In the above example the code is first tested with INIT0=1 to make sure that the code modification did not break anything. Then it is tested with INIT0=0. The use of HUGE will immediately trigger a floating point exception at runtime because Y needs to be initialized ; then this initialization is moved right where it is needed, and finally the code will read :

```
INIT0=-1
IF (INIT0 == 0) THEN
  ZVALUE=HUGE(1.)
ELSE
  ZVALUE=0.
ENDIF
IF (INIT0 >= 0) THEN
  X(:)=ZVALUE
ENDIF
DO J=1,N
  X(J)=F(J)
  Y(J)=0
```

```

Y (J) =Y (J) +X (J)
ENDDO

```

4 The problem of the extension zone for scalability

4.1 Gridpoint load imbalance

In order to limit the number of useless gridpoint computations in the physical parameterizations, the variable NGPTOT_CAP was created to stop the gridpoint computation at the point beyond which all the gridpoint of a task are in the extension zone.

Consequently the northern tasks are imbalanced, compared to the others (figure 1). While this choice was meaningful in the shared-memory model of the years 90, we should wonder if this is the proper choice in the distributed memory model of today.

Therefore a new namelist variable has been created (LGPTOT_CAP) in order to condition the use or not of this "capping" method.

The first benchmarks are rather in favour of not using the capping, though the signal is not very strong.

Note that if the capping is disabled (LGPTOT_CAP=.FALSE.) then the gridpoint norms of the fields looks different because the gridpoint norms are always computed over the whole area C+I+E.

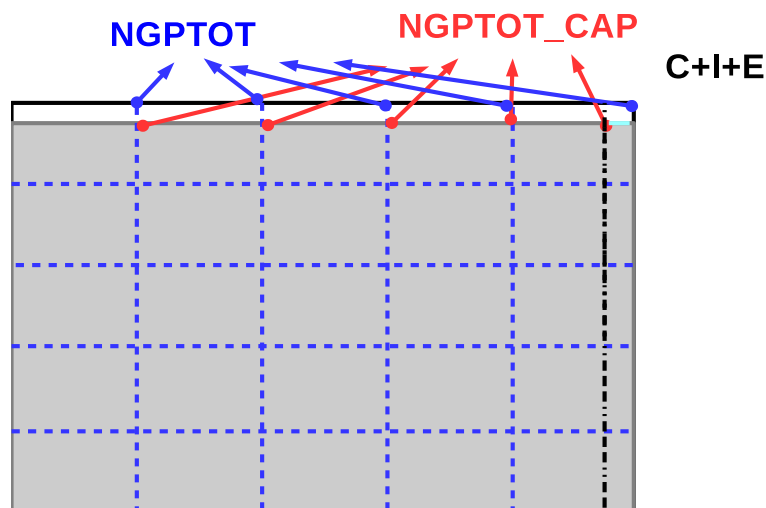


Figure 1: *Gridpoint areas of computation*

4.2 Semi-lagrangian failure

In theory, the model is able to run with up to such a number of MPI tasks that there would be one gridpoint per task (though in practice issues would raise before, in spectral space). However, far before this limit, the setup of the semi-lagrangian scheme aborts with this obscure message :

```

ABORT ! SLRSET: IFL IS OUT OF BOUNDS

```

The usual workaround is then to reduce the number of MPI tasks and increase the number of OPEN-MP threads instead, which is limited however, and which may not be the best for the computational performance.

Further investigations revealed that this abort, which has never been observed in the global model, is triggered by the semi-lagrangian halo of a task being fully inside the extension zone. Consequently, another workaround would be to increase the width of the halo, which is bad for the model scalability anyway. Actually it appears that the program always force the origin point of a semi-lagrangian trajectory to remain in the core area. Consequently, if the halo is fully inside the extension zone the origin point would eventually be moved outside the halo, and this triggers the abort (figure 2).

But since the values in the extension zone will be overwritten by the large scale data from coupling, the solution is just to force the points in the extension zone to remain in their halo, which is easily achieved by forcing these points to move along the X direction only (figure 3).

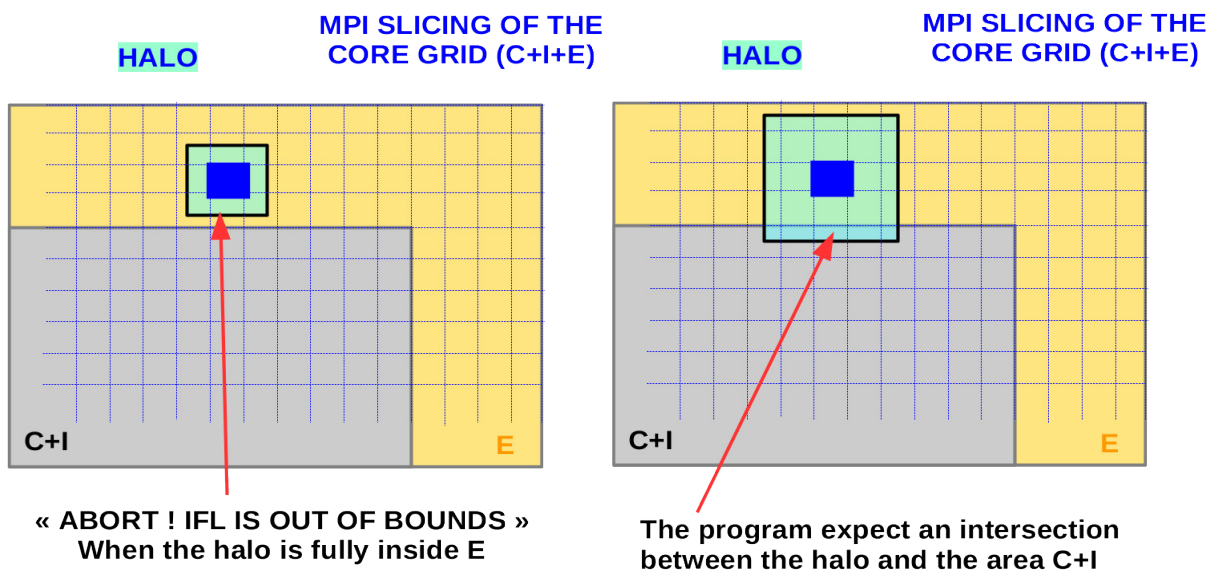


Figure 2: Condition of abort with the semi-lagrangian halo

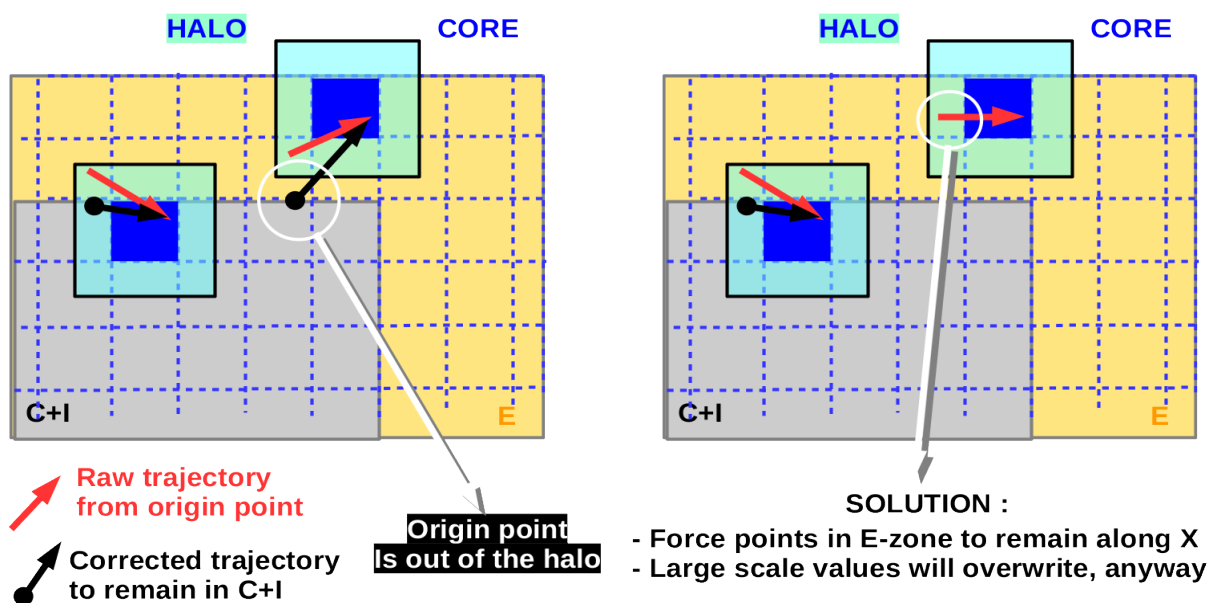


Figure 3: Origin and fix of the semi-lagrangian halo in the extension zone

5 Overall performance enhancements

The modifications described in the previous two sections (memory bandwidth, capping, and "slrset" issue) have been implemented on top of cycle 46T1, and Arome-France has been run up to 32400 MPI tasks. Actually, so many tasks were not enough for the "slrset" fix to be needed because the best performance is achieved with a distribution in gridpoint space along the two directions.

As pointed out during the talk, the semi-lagrangian computation on tasks fully in extension zone is useless ; but it was performed because the "capping" mechanism with NGPTOT_CAP was not used in this part of the code. The new flexible capping mechanism with LGPTOT_CAT is fixing this mistake.

The efficiency is clearly enhanced, by 8% to 12%. The "capping" mechanisms (LGPTOT_CAP=.TRUE.) should be preferred for a huge number of tasks because it slightly improves the scalability.

6 The load imbalance cause by the meteorology nature

A profiling of AROME shows that another big issue is the load imbalance of the physical parameterizations. This origin of this imbalance is in the nature of meteorology (the microphysics is particularly concerned since it is inactive where the sky is clear).

To reduce this load imbalance the natural solution is to reduce the number of MPI tasks and increase the number of OPEN-MP threads in order to take advantage of share-memory parallelism. But this technique is limited by the number of CPU cores in a computational node.

Nevertheless there might be another solution : since the data in gridpoint space are distributed in blocs of NPROMA gridpoints, we may consider to shuffle the NPROMA blocs of the most "expensive" tasks with those of the "cheapest" task. Overlapping the supplementary communications with the exchanged gridpoint computations is possible since the communications would be able to use the non-blocking protocol. Many strategies of re-shuffling are possible, from static ones (like balancing points over sea with points over land) to dynamic ones (load imbalance analysis at each time step).

The feasibility of that strategy should be studied.

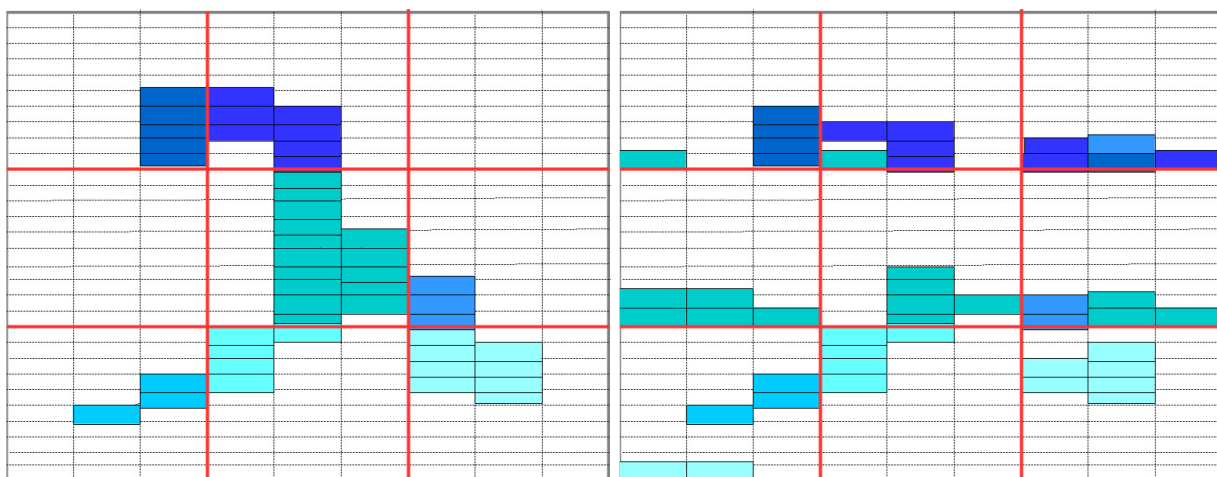


Figure 4: *load imbalanced of physics illustrated by a meteorologic perturbation over a model of 9 MPI tasks and 30 NPROMA blocs per task (left) ; and se same with re-shuffled blocs (right)*

Progress in turbulence, shallow convection and cloud microphysics in MetCoOp

Karl-Ivar Ivarsson

1 Introduction

There are some weaknesses in the model that have been addressed within the MetCoOp community during the last years. The reasons for those weaknesses are often complex and depends on several factors. The main focus of this paper is on those that least partly could be related to turbulence, shallow convection or to cloud microphysics. The complains are about:

- Too little of middle levels clouds.
- Too little precipitation from ‘moderate’ convective clouds.
- Too much fog, especially over sea and in spring.
- Too much low clouds in spring, but sometimes too little during other seasons.
- Missing supercooled rain.

The progresses examined in this paper come from several contributors and are the following:

- Update of HARATU (Wim de Rooy) during Autumn 2018. There are later updates that are yet not tested.
- Updates of fluxes over sea (Meteo France) within cycle 43, ECUME6.
- Model level thickness dependent VSIGQSAT. (MetCoOp)
- Modifications for better forecasts of supercooled rain. (MetCoOp)
- Modification of LTOTPREC option and of the Kain-Fritsch scheme. (MetCoOp)
- Increasing the value of XRIMAX. (Suggested by e.g. Eric Bazile)

The last modification, increasing XRIMAX is mainly tested after the all staff meeting and is only described briefly.

2 The results of the tests with the updates

Updates of the HARTU scheme

This update includes changes in the shallow convection scheme and in the turbulence scheme. The goal with this update is to increase the amount of middle level clouds, increase the precipitation from ‘moderate’ convective clouds and reducing excessive fog. Comparisons with large eddy simulation (LES) models indicate a more physical behaviour of the model with the updates included, compared to the original version.

A comparison has been made for three months, July and September 2017 and February 2018. The model version is cy40h.1.1.1 and the domain is the current one used by MetCoOp and covers north-western Europe.

The result is that the updated HARATU scheme leads to some increase middle levels clouds due to more efficient upward transport of heat and moisture in the boundary layer. This is seen for all three months. The scores show mainly neutral impact, but with a small improvement of the of the forecasts of clouds in especially February. There is no improvement of the forecasts of precipitation from ‘moderate’ convective cloud and there is no particular effect on the fog.

The frequency bias (FB) for cloud base for July 2017 is seen in figure 1. The lowest cloud base threshold also includes fog and is not changed with the new HARATU scheme, but there is a small increase of middle level clouds. The results for September and February are similar and are not shown.

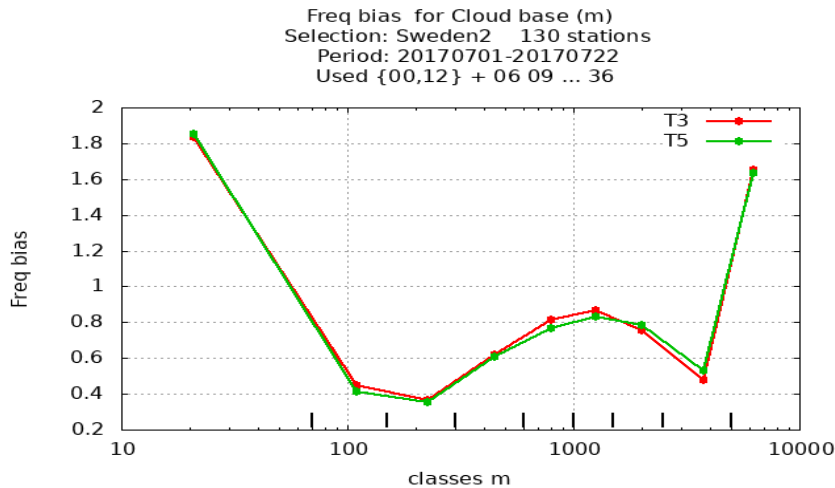


Figure 1: FB for different intervals of cloud base. The reference HARATU scheme in red and the updated in green. The cloud fraction should be at least 3/8 to be counted as a cloud base.

Updates of the fluxes over sea

In cycle 43 there is a possibility to use a new version of the ECUME scheme, ECUME6 in SURFEX. It is used for the surface fluxes over sea. The new version has been tested for April 2018 and September 2017 over the MeCoOp domain. Some case studies regarding fog in April 2019 are also made.

The fluxes of heat and moisture are a little enhanced with ECUME6, figure 2. The figure shows the differences of fluxes between ECUME6 and ECUME for April. The result for September 2017 is rather similar.

The increased fluxes lead to a slightly warmer and a little more moist lower troposphere.

The verification scores are mainly neutral. The case studies indicate that the occasions of fog in the model increases, which is unwanted since it is too much fog already. However, by combining ECUME6 with other updates described later in this paper, the result gets quite promising, but longer studies are needed to confirm this.

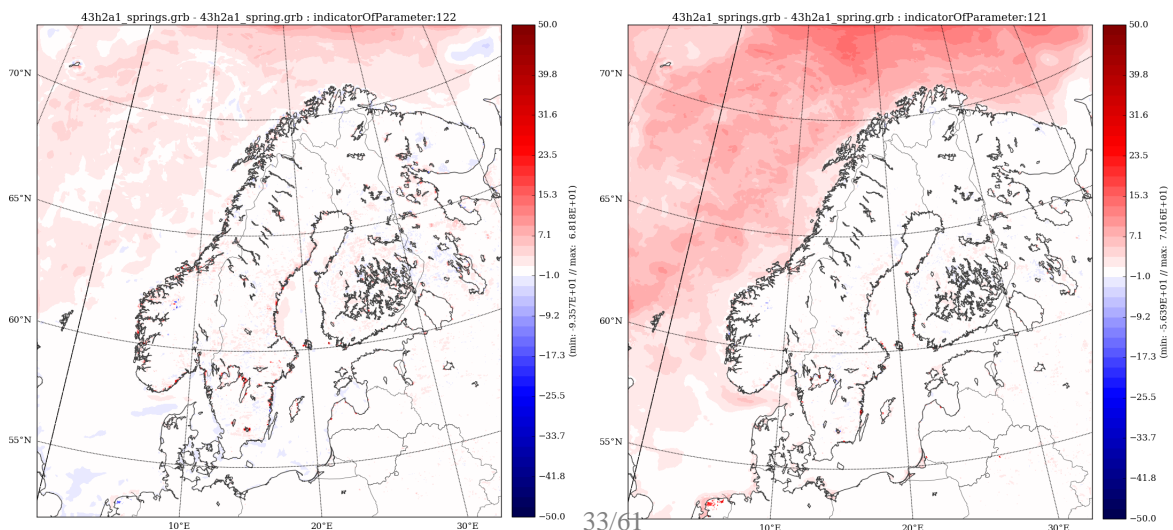


Figure2: The difference of fluxes for 6 hour forecasts during April 2018 between ECUME6 (new) and ECUME (old). The difference of sensible flux is to the left and the same difference for latent heat flux is to the right.

Model level thickness dependent VSIGQSAT

When a grid box gets larger, it is natural the the sub-grid scale variation of relative humidity gets larger also. Especially, in a vertically well-mixed layer the vertical increase of relative humidity is usually about 4 to 5 % per 100 metre. This also means that in a such layer of 200 metre depth with a mean relative humidity of 97%, there should be a saturated upper part, but not if the layer is 100 metre deep only. One has to keep in mind that a layer is of course not always well-mixed and there is also a horizontal variation in a grid box.

Here, VSIGQSAT is unaltered for a fix model level thickness (30 m) only. If other cases it is set to $VSIGQSAT \times \Delta Z/30$, where ΔZ is the level thickness. The range of $\Delta Z/30$ is limited to [0.5:1.5]. With the current 65 levels and $VSIGQSAT = 0.03$, the modified VSIGQSAT becomes 0.015 at the lowest model level, not changed around 200m and 0.045 above 400m.

This modification has been tested with same area and the same test periods (July and September 2017, February 2018) as for the HARATU test. The result is mainly neutral with respect to the scores, but the excess of fog is reduced, and the forecasts of cloud base are improved, see figure 3, showing the result for February 2018. The FB of the lowest threshold indicate that there is still too much fog. The results for July and September 2017 look quite similar, not shown.

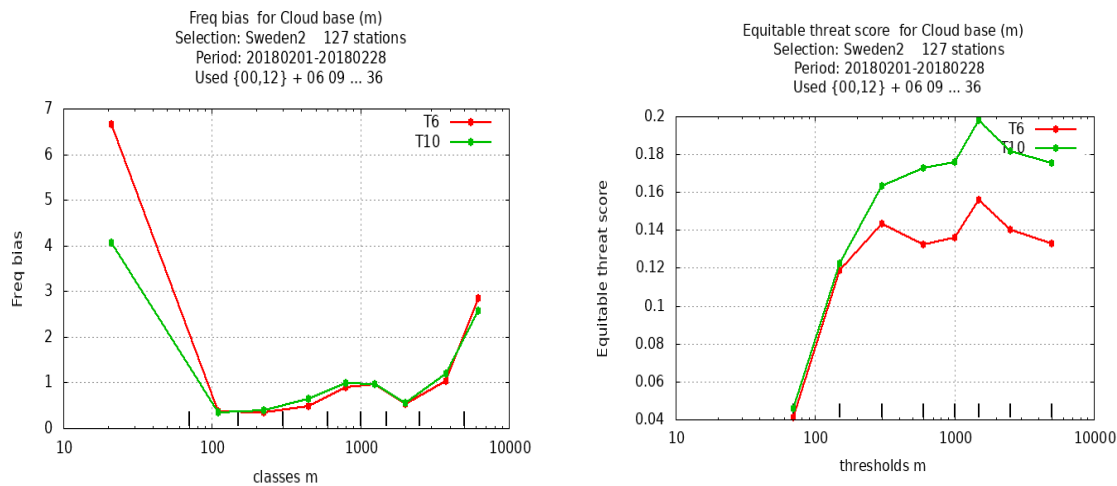


Figure 3: The reference run in red and model level thickness dependent VSIGQSAT in green. The cloud fraction should be at least 3/8 to be counted as a cloud base. To the left is FB for different intervals of cloud base and to the right is the ETS (equitable treat score) for different thresholds of cloud base.

Modifications for improving forecasts of supercooled rain

In 2017 an update for improving supercooled rain was introduced. This was achieved by skipping conversion of supercooled rain into snow and to use higher thresholds for the mixing ratios of water species and for the ice nucleus concentration in some parametrizations of the conversion of water species into graupel. Those changes work well in many situations, but unfortunately not always. One such event was in February 22 this year over northern Sweden. The model produced only small amount of supercooled rain, most of it was graupel. In reality there was supercooled rain only in most places.

Two different solutions for improvement are found. The simplest one is just to increase two of the thresholds by a factor of ten. This means increasing RFRMIN(3) and RFRMIN(4) to 3.0E-6 instead of 3.0E-7. But the most efficient way found is to include thresholds for cloud ice and cloud water in the processes controlled by RFRMIN(3) and RFRMIN(4). One example of this is seen in figure 4.

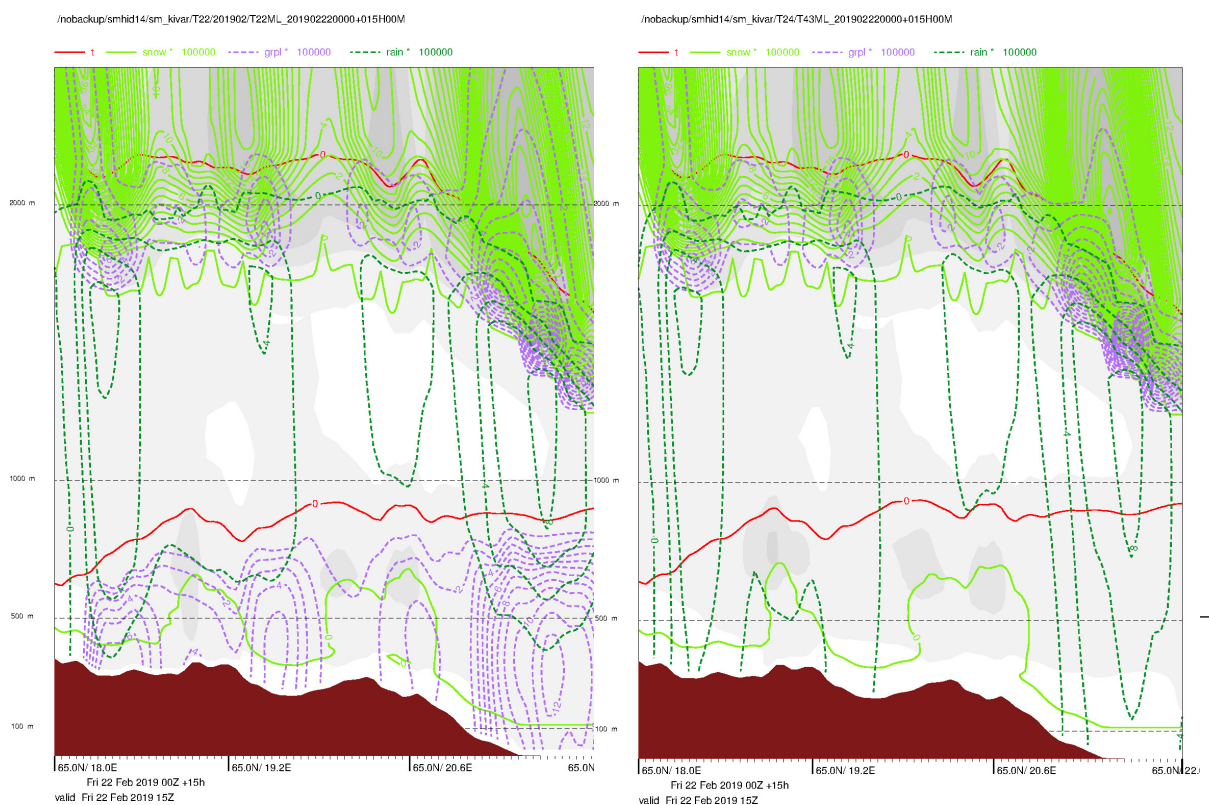


Figure 4: Cross sections 18-22E and 65N for forecasts issued 2019022200 and forecast length 15 h. Red line is isotherm for 0 C showing temperature above freezing from 600-900m up to about 2000m. Light green solid lines are isolines for mixing ratio of snow, dashed purple lines are isolines for mixing ratio of graupel and dark green solid lines are isolines for mixing ratio of rain. To the left: Original set up. To the right: Thresholds for cloud ice and cloud water I included.

With the reference version, rain is converted to graupel in the area near ground where temperatures are below freezing. With thresholds for cloud condensate included for the processes turning cloud condensate, rain and snow into graupel, there is much less graupel and more supercooled rain which agrees with observations.

Before putting it into operation one has to check that these changes have no undesired side-effects.

Modifications of LTOTPREC option and test of the Kain-Fritsch scheme

With the LTOTPREC. option, the convective precipitation in the EDMF scheme does not reach the ground instantaneously. Instead it advects vertically and horizontally and interacts with microphysics before reaching ground. But the convection and thus also the precipitation become more intense, since a larger fraction of the grid box is assumed for convection. An alternative is to use the same fraction also with LTOTPREC. The verification scores show very little impact (compared to using LTOTPREC = F) except that the FB of precipitation becomes somewhat better. But it is still too little precipitation from 'moderate' convective clouds.

A scheme for deep convection, the Kain-Fritsch scheme, exist in the AROME physics, but is seldom or never used. It has also been tested in order to increase precipitation from 'moderate' convective clouds. Some bug fixes and an adaptation for high horizontal resolution where needed in order to get it working. Although working technically well, none of the weaknesses discussed here seems to be solved by it so far.

Increasing the value of XRIMAX.

XRIMAX is used in SURFEX for tuning the exchange between the surface and the lowest model level. Theoretically, the value should be infinity, but earlier tests showed that such a low value as zero was the best. But the model has developed, and recent tests indicate that XRIMAX should be retuned. It should probably be increased to at least 0.2, since this seems to solve some of the problems with too much fog. A higher XRIMAX leads to less fog when the fog is caused by vertical mixing but existing fog may be more persistent. Case studies indicate that the former effect dominates, but longer tests are needed. A possible undesired effect noticed by Mariken Holmleid is that the 2m- temperature occasionally gets too low over some coastal areas when a larger XRIMAX is used.

4 A short summary

The result from the different progresses examined here can be summarized as follows:

- Update of HARATU during Autumn 2018: A small improvement of the forecasts of middle levels clouds, mainly neutral impact in other respects.
- Updates of fluxes over sea within cycle 43, ECUME6: Increased fluxes of heat and moisture over sea. Mainly neutral impact of the scores. Increased amount of fog over sea.
- Model level thickness dependent VSIGQSAT: Somewhat improved forecasts of middle levels clouds and a reduction of fog. But still too much fog.
- Modifications for better forecasts of supercooled rain: Seems to work well, but more tests needed, especially for searching possible side effects.
- Modification of LTOTPREC option and of the Kain-Fritsch scheme: Small improvement of the FB for rain with the modified LTOTPREC. So far no clear improvement with the Kain-Fritsch scheme.
- Increasing the value of XRIMAX: Seems to reduce fog, but may deteriorate the T2m forecasts in coastal regions.

'SLX' verification scheme (Structure of Local eXtremes)

Bent Hansen Sass

1 Introduction

SLX is the short abbreviation for 'Structure of Local eXtremes'. SLX is a new verification scheme for use in NWP, describing the degree of match between a forecast field, normally 2-dimensional, and a corresponding observation field (analysis), having emphasis on local extremes of these spatial fields. It takes into account a neighborhood size to match the occurrence of local extremes. The SLX is currently developed for precipitation. Thus the results will depend on a selected precipitation accumulation period.

It is easy to mention motivations for developing a NWP verification scheme that quantifies the model's ability to predict local extremes. First of all, the NWP model output may need to provide answers to the following questions:

'What will be the extreme values of a given weather parameter for today?' - and 'where will the extremes be located geographically?' In order to maintain a realistic communication on these issues with users of NWP, e.g. duty forecasters, based on objective verification of NWP, we apparently need a scheme dedicated to measure the ability of the NWP model to predict local extremes.

The SLX scheme is including spatial uncertainty in the verification process. This is necessary for modern verification schemes which need to consider the 'double penalty issue', mentioned widely in recent years due to the problem of matching high resolution forecasts with analyses in individual points (e.g. Sass and Yang 2012). In order to treat temporal accuracy the scheme should be run for different accumulation periods.

Gilleland et al. (2010) makes a classification of different types of spatial verification techniques: Four types are mentioned: neighborhood, scale separation, features based, and field deformation. It is most natural to place the SLX scheme into the first group. Also the well known fractions skill score (Roberts and Lean 2008) belongs to this group.

Precipitation is particularly interesting to verify when considering local extremes since a large variability of observed or diagnosed precipitation has been documented, e.g. Eggert et al. (2015) investigating temporal and spatial scaling impacts on extreme precipitation over Germany. Fiener and Austerwald (2009) documented a variability of observed precipitation down to sub-km scales. This emphasizes the large observed variability of precipitation which should be compared with model predictions at different spatial and temporal scales.

The relevance of developing SLX increases further in these years in view of expected larger extreme values of precipitation in a future warmer climate, e.g. Scoccimarro and Gualdi (2013), Bao et al. (2017) and Witze (2018).

2 Computational procedure

The computational procedure of SLX is illustrated in Fig.1. The figure illustrates that the computational scheme determines an observed (analyzed) minimum (OB-min), and forecasted minimum (FC-min) respectively. Correspondingly, analyzed and forecasted maxima, OB-max and

FC-max, respectively, are determined. A challenge may occur that exactly the same minimum value or maximum value may occur a multiple number of times over the computational area, e.g. in the case of zero minimum precipitation. All such points are in principle equally valid as an extreme point. The scheme keeps track of all points. In the case of many equal points an algorithm allows to carry out computations for a (large) arbitrary subset of extremes. The scheme also allows that a minimum closest to a value larger than zero is searched for. This may be relevant if zero precipitation is not so important in the actual application. For each local extreme a squared environment of grid points are kept track of. The dimension N defines the size of the neighborhood.

Also a boundary zone having B number of grid points is defined in order to allow the same number of internal points of the computation procedure, for small- up to the largest considered neighborhoods.

Fig.1 represents either the full model domain or a sub-domain. The algorithm is designed such that the total domain may be divided into a given number of sub-domains defined by a number of grid points in each coordinate direction. For large model areas of, say 500 or more grid points in each coordinate direction, this is advisable in order to distinguish regional differences of the computations. However, currently the results over sub-areas are averaged to form a result applicable to the entire model domain. SLX is a weighted average between components describing match of minima and maxima, using analyses and forecasts of the field. The individual components illustrate specific properties of the forecast versus analysis.

$$SLX = \frac{1}{4} (SLX_{ob-max} + SLX_{ob-min} + SLX_{fc-max} + SLX_{fc-min})$$

$$SLX_{ob-max} = S (P_{ob-max}, P_{fe-max}/P_{ob-max}), \quad P_{fe-max} = \text{Max}\{ P_{fe}(i, j, \tau) \}, \quad (ob-max) \\ 0 < \tau \leq \tau_m, \quad i \in [1, \dots, N], \quad j \in [1, \dots, N] \quad (1)$$

$$SLX_{ob-min} = S (P_{ob-min}, P_{fe-min}/P_{ob-min}), \quad P_{fe-min} = \text{Min}\{ P_{fe}(i, j, \tau) \}, \quad (ob-min) \\ 0 < \tau \leq \tau_m, \quad i \in [1, \dots, N], \quad j \in [1, \dots, N] \quad (2)$$

$$SLX_{fc-max} = S (P_{fc-max}, P_{oe-max}/P_{fc-max}), \quad P_{oe-max} = \text{Max}\{ P_{oe}(i, j, \tau) \}, \quad (fc-max) \\ 0 < \tau \leq \tau_m, \quad i \in [1, \dots, N], \quad j \in [1, \dots, N] \quad (3)$$

$$SLX_{fc-min} = S (P_{fc-min}, P_{oe-min}/P_{fc-min}), \quad P_{oe-min} = \text{Min}\{ P_{oe}(i, j, \tau) \}, \quad (fc-min) \\ 0 < \tau \leq \tau_m, \quad i \in [1, \dots, N], \quad j \in [1, \dots, N] \quad (4)$$

S is a score function between zero and 1 shown in Fig.2. Higher values means higher quality, with 1 valid for a perfect forecast. S is a decreasing function with increasing difference of absolute value between between forecast and analysis. Currently the piecewise linear and asymmetric function of the Fig. 2 is used. Asymmetry has implications for the SLX computations compared with a symmetric function.

The P_{fe} and P_{oe} -functions in (1) –(4) describe in each case the precipitation variability, forecasted and observed respectively, in the neighborhood of the extreme value (ob-max, ob-min, fc-max, fc-min respectively). τ is the actual precipitation accumulation time used in the computations. τ_m is the maximum possible choice. S depends on the extreme value parameter and the ratio between the P_{fe} - and P_{oe} -functions and the extreme value parameter. The current choice is that $S = 1$ for small precipitation amount $P \leq k$ to be verified (see Fig.2). The score function could be chosen flexible depending on the User Community involved.

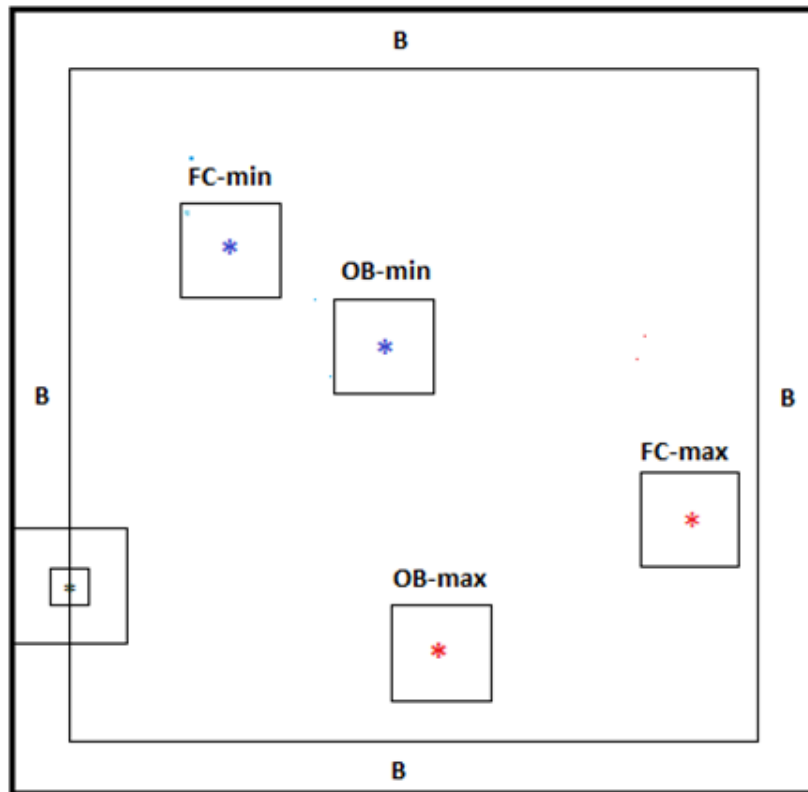


Figure 1: Concept of verifying local extremes in neighborhoods around observed local minima (OB-min), local observed maxima (OB-max), local forecasted minima (FC-min) and local forecasted maxima (FC-max), respectively. A boundary zone is introduced in order to allow the same number of internal points of the computation procedure for small- up to largest considered neighborhoods.

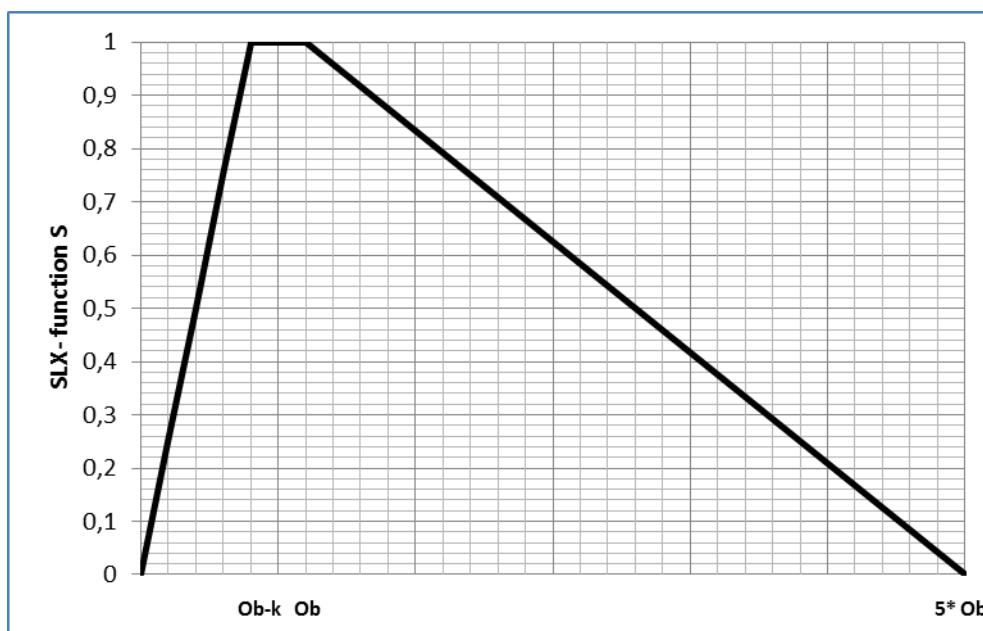


Figure 2: The score function S is a function of observed value and fraction between forecasted and observed value.

3 Results

The SLX verification is currently being tested in both idealized tests and tests simulating verification in operational conditions. A report which is being prepared for a journal will include a documentation of these tests. The results of current tests indicate that the scheme takes into account 'double penalty' issues as expected, e.g. the effect of small scale numerical noise and displacements of forecasted local extremes in the neighborhood size considered. Horizontal displacements of larger precipitation systems, e.g. frontal precipitation bands also appear to be treated well.

The fact that the combined output of SLX components includes both local maxima and minima makes it robust, e.g. it will tend to penalize model bias. The SLX scheme is an extension of the scheme by Sass and Yang (2012) based on locations of extreme observations. SLX includes full field comparisons and also a diagnosis of analysis field around forecasted local extremes. In this way systematic over- and under forecasting in specific regions can be diagnosed. An important property of the scheme is that the score function can be chosen flexible, e.g. as a consequence of a dialogue between developers and the user community.

4 References

- Bao, Jiawei , Steven C. Sherwood, Lisa V. Alexander and Jason P. Evans , 2017: Future increases in extreme precipitation exceed observed scaling rates, *Nature Climate Change*, 7 (10.1038/nclimate3201)
- Eggert, B., P.Berg, J.O. Haerter, D. Jacob and C. Moseley , 2015: Temporal and spatial scaling impacts on extreme precipitation , *Atmos. Chem. Phys.* , 15, 5957 -5971.
- Fiener, P. and K. Austerwald, 2009: Spatial variability of rainfall on a sub-kilometre scale. *Earth Surf. Process. and Land forms* , 34, 848-859
- Gilleland, E., D.A. Ahijevych, B.G. Brown and E.E. Ebert, 2010: Verifying Forecasts Spatially. *Bull. Amer.Meteor. Soc.*, October, 1365 – 1373.
- Roberts N.M. and H.W. Lean, 2008: Scale-selective verification of rainfall accumulations from high-resolution forecasts of convective events. *Mon. Wea. Rev.*,136, 78-97.
- Sass, B.H. and X. Yang, 2012: A verification score for highresolution NWP : Idealized and preoperational tests. *HIRLAM Tech. Rep. No 69, 28 pp, Dec. 2012*, [Available from www.hirlam.org]
- Scoccimarro, E. and S. Gualdi, 2013: Heavy Precipitation Events in a warmer climate : Results from CMIP5 models , *J. Cli.* , <https://doi.org/10.1175/JCLI-D-12-00850.1>
- Witze, A. 2018: Why extreme rains are getting worse : *Nature*, Vol. 563 , Nov 2018

Modelling Flow-Dependent Covariances with Gaussian Integrals

Carlos Geijo, Spanish Meteo. Agency, AEMET; cgeijog@aemet.es

1 Introduction

Introducing flow-dependency in NWP analyses is necessary in order to better represent the actual state of the atmosphere in the initial conditions for a weather forecast. Currently, widely used methods to achieve this goal are DA by ensembles and variational algorithms like 4D-VAR. Here a new method is presented that has the appealing properties of being easy to implement and well suited for applications demanding a very high update frequency (e.g. Very Short Range NWP or NWP-NWC).

2 The Analysis Increments as a Gaussian Random Field on a Grid

The analysis increments Δ on an N-grid can be considered a Gaussian Random Field with a source term S. This statement follows immediately from a reorganization of the terms in the 3D-VAR cost function

$$2J_{3DVAR}(\Delta, y) = \Delta^T B^{-1} \Delta + (y - \Delta)^T R^{-1} (y - \Delta) = \Delta^T G^{-1} \Delta - 2\Delta^T S + y^T R^{-1} y \Rightarrow \\ \Rightarrow 2J_S(\Delta) = \Delta^T G^{-1} \Delta - 2\Delta^T S \quad (1)$$

with

$$G^{-1} \equiv B^{-1} + R^{-1} \quad ; \quad S \equiv R^{-1} y = R^{-1} (ob - fg)$$

where the last term quadratic in the observation increments “(ob-fg)” in (1) has been disregarded. This amounts to consider the observation increments set as a non-random field. The source field S is just given by these increments after being duly normalized. The analysis problem becomes that of finding the Δ that maximizes the probability conditioned on a given set of observation increments :

$$P(\Delta, y) \propto e^{-J_{3DVAR}} = e^{-\frac{1}{2}\Delta^T G^{-1} \Delta + \Delta^T S} e^{-\frac{1}{2}y^T R^{-1} y} \equiv e^{-J_S(\Delta)} e^{-\frac{1}{2}y^T R^{-1} y} \propto P(\Delta|y) P(y)$$

and P(y) can be absorbed in the normalization, which is the so-called generating function N(S)

$$P(\Delta|y) \equiv P_S(\Delta) = \frac{e^{-J_S(\Delta)}}{N(S)} \quad ; \quad N(S) = \int d\Delta_1 \dots d\Delta_N e^{-J_S(\Delta)} = \sqrt{(2\pi)^N \|G\|} e^{\frac{1}{2}S^T GS}$$

2.1 3D-VAR Results Recovered from this Formalism

The analysis is obtained by expectation of Δ as given by $P_S(\Delta)$

$$\langle \Delta_i \rangle_S = \frac{1}{N(S)} \int d\Delta_1 \dots d\Delta_N \Delta_i e^{-J_S(\Delta)} = \frac{1}{N(S)} \frac{\partial}{\partial S_i} N(S) = \frac{1}{2} [G_{ij} S_j + S_j G_{ji}] = G_{ij} S_j = \langle \Delta_i \Delta_j \rangle_{S=0} S_j \quad (2)$$

where the last equality follows from the well-known property of Gaussian Integrals for G symmetric and positive definite

$$G_{ij} = \frac{1}{N(S=0)} \int d\Delta_1 \dots d\Delta_N \Delta_i \Delta_j e^{-\frac{1}{2} \Delta^T G^{-1} \Delta} = \frac{1}{N(S=0)} \int d\Delta_1 \dots d\Delta_N \Delta_i \Delta_j e^{-J_{S=0}(\Delta)}$$

In a similar way, one can see that the analysis error at grid point “i” is

$$\langle \Delta_i^2 \rangle_S - \langle \Delta_i \rangle_S^2 = \langle \Delta_i^2 \rangle_{S=0} = G_{ii}$$

These results are not surprising as soon as we notice that $G^{-1} = (B^{-1} + R^{-1})$ is indeed the Hessian of the 3D-VAR problem, that is, the inverse of the 3D-VAR analysis covariance error matrix, frequently denoted by A^{-1} . The connection between the 3D-VAR algorithm and this Gaussian Integral (GI) formalism is explored further in section 4 after we next introduce a computation scheme by expansion in power series.

2.2 The Error Covariance G as Green Function. Analogy with QFT Propagators.

It is possible to make a close analogy between the calculation of the 3D-VAR solution just outline above, and common methods employed in the theory of random fields (QFT Quantum Field Theory) for the calculation of probability amplitudes for different fundamental physical processes (scattering cross sections, etc...). This analogy arises from thinking of the covariance matrix G as a kind of Green Function or, in QFT terminology, as a kind of propagator. This correspondence is just the reverse of that presented in [1],[2], where the similitudes between the Green Function for a variational constrained problem and covariance matrices were emphasized.

One immediate application of this idea is to consider the possibility of introducing external fields in the formalism, as is done in QFT when, for instance, one wants to take into account the effect of an ambient electromagnetic field in the correction to the energy levels of an atom. In the case of interest here, we may introduce a \mathbf{V} vector field that converts the correlation function (or “2-point function” in QFT parlance) in a functional of this \mathbf{V} field

$$\langle \Delta_i \Delta_j \rangle_{S=0} [\bar{\mathbf{V}}] \propto \int d\Delta_1 \dots d\Delta_N \Delta_i \Delta_j \exp\left(-\frac{1}{2} \Delta^T G^{-1} \Delta - \frac{\mu}{2} \text{tr}\left([\bar{\mathbf{V}} \square \bar{\nabla} \Delta][\bar{\mathbf{V}} \square \bar{\nabla} \Delta]^T\right)\right) ; \quad \text{dim}(\mu) = \left[\frac{\text{error}}{\text{time}}\right]^{-2} \quad (3)$$

one can say that the “free propagation” or “kinetic energy” of the error field ($\frac{1}{2} \Delta^T G^{-1} \Delta$) is corrected by an “interaction with a background \mathbf{V} field” with coupling factor μ .

3 Implementation of a Computation Algorithm and First Tests

The calculation proposed in (3) can be approximated by a power series in μ . With $\mathbf{V}_p = (\mathbf{u}_p, \mathbf{v}_p, \mathbf{w}_p)$

$$\langle \Delta_i \Delta_j \rangle_{S=0} [\bar{V}] \square \int d\Delta_1 \cdots d\Delta_N \exp\left(-\frac{1}{2} \Delta^T G^{-1} \Delta\right) \Delta_i \Delta_j \left[1 - \frac{\mu}{2} \sum_{p \in (1, \dots, N)} (\bar{V} \cdot \nabla \Delta)_p^2 + O(\mu^2)\right] = \langle \Delta_i \Delta_j \rangle_{S=0} - \frac{\mu}{2} \sum_{p \in (1, \dots, N)} u_p^2 \langle \Delta_i \Delta_j (\partial_x \Delta)_p^2 \rangle_{S=0} + \dots$$

and the derivatives of analysis increments are approximated with finite differences on the grid. The result is that the correction to first order in μ is given by a sum over all the grid points of four-moment values, with this sum modulated by the \mathbf{V} field:

$$\sum_{p \in (1, \dots, N)} \left(\frac{u_p}{\Delta x}\right)^2 \langle \Delta_i \Delta_j (\Delta_{p(x)+1} - \Delta_{p(x)-1})^2 \rangle_{S=0} + \dots = \sum_{p \in (1, \dots, N)} \left(\frac{u_p}{\Delta x}\right)^2 \left(\langle \Delta_i \Delta_j \Delta_{p(x)+1}^2 \rangle_{S=0} + \langle \Delta_i \Delta_j \Delta_{p(x)-1}^2 \rangle_{S=0} - 2 \langle \Delta_i \Delta_j \Delta_{p(x)+1} \Delta_{p(x)-1} \rangle_{S=0} \right) + \dots$$

These four-moment are in turn given by the matrix elements of G , because by Wick's rule

$$\langle \Delta_a \Delta_b \Delta_c \Delta_d \rangle_{S=0} = G_{ab} G_{cd} + G_{ac} G_{bd} + G_{ad} G_{bc}$$

These calculations let themselves be nicely represented by diagrams (the famous Feynman's diagrams), but the number of terms becomes quickly very high. For instance, for a 3-D \mathbf{V} field, to order μ we must sum over 21 four-moments, and to order μ^2 the sum is over 126 six-moments (10 and 35 respectively if we are satisfied with a 2-D \mathbf{V} field). As each four-moment gives 3 products of pairs of G matrix elements and a six-moment gives 15 products of pairs, we have 63 of such products to order μ and 1890 to order μ^2 , to be sum over all grid points. This vast amount of computations can be dramatically reduced by using the fact that G is sparse (covariances of analysis errors decay with grid point separation).

A first implementation has been utilized to evaluate the potential of this technique, both in terms of its impact on the analysis and also on its feasibility given a certain amount of computation power. The algorithm scales well with the number of observations: it is not necessary to compute these "2-point functions" for all pairs of grid points, is just enough to carry it out only for each observation.

Below these lines, the deformation of an isotropic correlation (contoured on the left bottom corner) due to a vortex is shown (fig 1). On figure 2 the modulation caused by a HARMONIE-AROME wind field at level 55 on an isotropic correlation with length scale characteristic for the specific humidity variable is shown. This test with a 2-D \mathbf{V} field and to order μ gave a processing time of about 1 sec/observation.

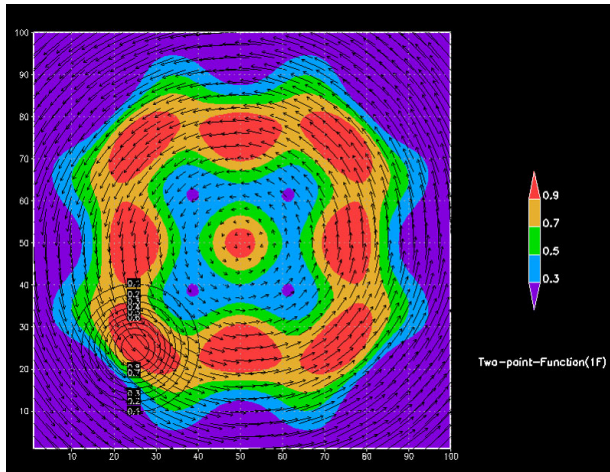


Figure 1: Correlations from 9 observations located in a vortex. Isotropic correlation for the one at the bottom-left is shown in contours, its length scale is 10 grid points.

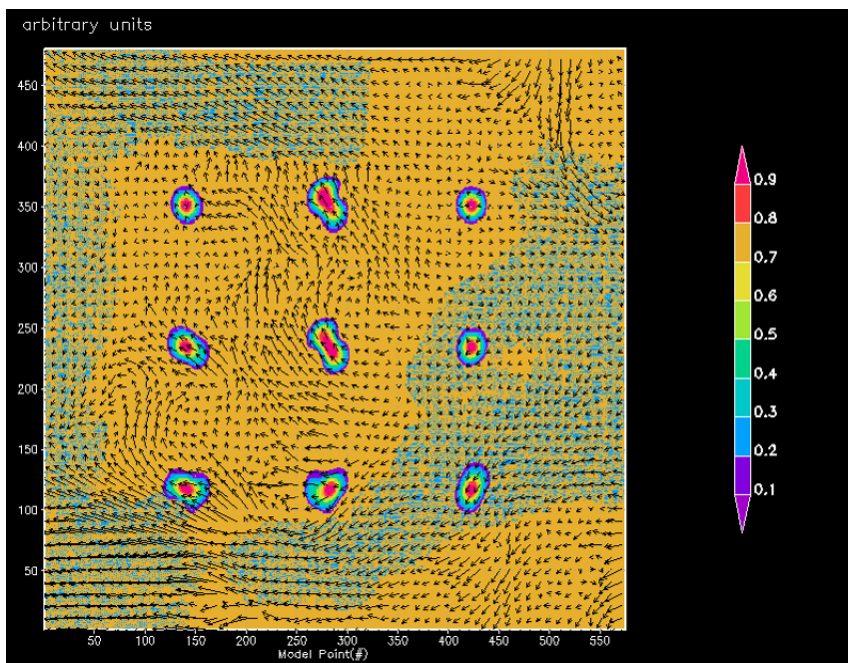


Figure 2: Horizontal correlation functions for 9 specific humidity (q) observations on an atmospheric level about 850hPa over the Iberian Peninsula, derived by coupling isotropic error correlations to the model wind field. The length scale of these isotropic correlations is determined from actual model errors.

4 Approximation to the 3D-VAR Solution with Gaussian Integrals

The 3D-VAR solution as given in (2) can be approximated by GI by decomposing the G propagator in a B propagator and a perturbation produced by the spatial distribution and correlations among the observations represented by R^{-1} . This perturbation is given in model space (R^{-1} is actually $H^T R^{-1} H$,

but the simpler notation is retained for comfort). R may not exist, but this is not a problem as it is not required for the calculations that follow. Indeed, R^{-1} will have, when represented on the grid, many zeros, which actually is an advantage to reduce the number of required computations !.

The generating function

$$N_G(S) = \sqrt{(2\pi)^N \|G\|} e^{\frac{1}{2} S^T G S} \quad (4)$$

can be computed for small R^{-1} by expanding in powers of it

$$N_G(S) \approx \int d\Delta^N e^{-\frac{1}{2} \Delta^T B^{-1} \Delta + \Delta^T S} \left(1 - \frac{1}{2} \Delta^T R^{-1} \Delta + \frac{1}{8} (\Delta^T R^{-1} \Delta)^2 + O(R^{-3}) \right) = N_B^0(S) (1 + N_B^1(S) + N_B^2(S) + \dots)$$

where the subscripts ‘‘G’’ and ‘‘B’’ have been introduced to distinguish the ‘‘free propagator’’ employed in each case. Here

$$N_B^0(S) = \sqrt{(2\pi)^N \|B\|} e^{\frac{1}{2} S^T B S}; \quad N_B^1(S) = -\frac{1}{2} \left(Tr(BR^{-1}) + S^T (BR^{-1}B) S \right)$$

$$N_B^2(S) = \frac{1}{8} \left(Tr(BR^{-1}) + S^T (BR^{-1}B) S \right)^2 + \frac{1}{2} \left(\frac{1}{2} Tr(BR^{-1}BR^{-1}) + S^T (BR^{-1}BR^{-1}B) S \right)$$

These results can also be obtained more directly from (4) by making use of the ‘‘Neumann series’’ for G (see footnote), valid for linear bounded operators. This is always the case for operators on finite dimensional space, although convergence is not guaranteed.

$$G = (1 + BR^{-1})^{-1} B = B(1 + R^{-1}B)^{-1} \approx B - BR^{-1}B + BR^{-1}BR^{-1}B + \dots \quad (5)$$

and the following relation between determinant and trace of a matrix

$$\ln \|M\| = Tr(\ln M) \quad ; \quad M = 1 + BR^{-1} \equiv 1 + \varepsilon \quad ; \quad \ln M = \varepsilon - \frac{\varepsilon^2}{2} + O(\varepsilon^3)$$

so that

$$N_G(S=0) \approx N_B^0(S=0) \left(1 - \frac{1}{2} Tr \varepsilon + \frac{1}{8} (Tr \varepsilon)^2 + \frac{1}{4} Tr \varepsilon^2 + O(\varepsilon^3) \right)$$

or up to the ε^2 order

$$N_G(S=0) \approx N_B^0(S=0) e^{-\frac{1}{2} (Tr \varepsilon - \frac{Tr \varepsilon^2}{2})}$$

Now, the quantity that we need to compute is, according to (2):

(footnote) Thank you to Roel Stappers for pointing out to me this formal solution for the 3D-VAR analysis

$$\begin{aligned}
\langle \Delta_i \Delta_j \rangle_{G,S=0} &\approx \frac{1}{N_G(S=0)} \int d\Delta^N \Delta_i \Delta_j e^{-\frac{1}{2} \Delta^T B^{-1} \Delta} \left(1 - \frac{\Delta^T R^{-1} \Delta}{2} + \frac{(\Delta^T R^{-1} \Delta)^2}{8} + \dots \right) = \\
&\frac{e^{\frac{1}{2} \left(Tr \varepsilon - \frac{tr \varepsilon^2}{2} \right)}}{N_B(S=0)} \int d\Delta^N \Delta_i \Delta_j e^{-\frac{1}{2} \Delta^T B^{-1} \Delta} \left(1 - \frac{\Delta^T R^{-1} \Delta}{2} + \frac{(\Delta^T R^{-1} \Delta)^2}{8} + \dots \right) = \\
&e^{\frac{1}{2} \left(Tr \varepsilon - \frac{tr \varepsilon^2}{2} \right)} \left(\langle \Delta_i \Delta_j \rangle_{B,S=0} - \frac{1}{2} \langle \Delta_i \Delta_j \Delta^T R^{-1} \Delta \rangle_{B,S=0} + \frac{1}{8} \langle \Delta_i \Delta_j (\Delta^T R^{-1} \Delta)^2 \rangle_{B,S=0} + \dots \right) = \\
&e^{\frac{1}{2} \left(Tr \varepsilon - \frac{tr \varepsilon^2}{2} \right)} \left(B_{ij} \left(1 - \frac{1}{2} Tr \varepsilon + \frac{1}{8} (Tr \varepsilon)^2 + \frac{1}{4} Tr \varepsilon^2 + O(\varepsilon^3) \right) - (BR^{-1}B)_{ij} \left(1 - \frac{1}{2} Tr \varepsilon + O(\varepsilon^2) \right) + \right. \\
&\quad \left. (BR^{-1}BR^{-1}B)_{ij} (1 + O(\varepsilon)) + \dots \right) = \\
&(B_{ij} (1 + O(\varepsilon^3)) - (BR^{-1}B)_{ij} (1 + O(\varepsilon^2)) + (BR^{-1}BR^{-1}B)_{ij} (1 + O(\varepsilon)) + \dots)
\end{aligned}$$

which is the 3D-VAR solution as given by (5) to second order in R^{-1}

5 References

- [1] C. Geijo and B. Escribá: “Variational Constraints for Data Assimilation in ALADIN-NH Dynamics”. 11th ALADIN-HIRLAM Newsletter, Aug. 2018 . <http://www.umr-cnrm.fr/aladin/IMG/pdf/nl11.pdf> also available in: https://www.researchgate.net/publication/326479446_Variational_Constraints_for_Data_Assimilation_in_ALADIN-NH_Dynamics
- [2] C. Geijo: “ANNEX to Variational Constraints for DA in ALADIN-NH dynamics”, Aug 2018 https://www.researchgate.net/publication/327117950_ANNEX_to_Variational_Constraints_for_DA_in_ALADIN-NH_Dynamics

A comparison of datamining tools: visibility estimation from AROME-Morocco outputs by Machine Learning regression

Driss BARI ⁽¹⁾ and Mohamed AMEKSA ⁽²⁾

¹DMN, CNRMSI/SMN, Casablanca, Morocco

² University Hassan II, ENSAM, Casablanca, Morocco

1 Introduction

Low visibility has been a challenge for weather forecasters for a long time, due to its negative impact on air, sea and road traffic. Indeed, the human and financial losses attributable to reduced visibility become increasingly important; hence, a good forecast of horizontal visibility is of great benefit to meteorological forecasters. So, to cope with this challenge in the area of numerical weather prediction, the potential of Datamining techniques to estimate horizontal visibility has been evaluated in several scientific studies.

Bartoková et al. (2015) have used the WEKA¹ platform to predict the occurrence of some classes of reduced visibilities. The authors developed a decision tree model to predict fog events in the coastal desert area of Dubai, United Arab Emirates. Bari and El Khelifi (2015) developed neural-network based models for LVP (Low Visibility Procedure) conditions at Nouasseur airport, Casablanca, Morocco using the packages (nnet) under the open source platform R². The authors used resilient back propagation neural networks as a learning algorithm. Kneringer et al. (2018) have used the `glm()` package under R platform for the development of an ordered logistic regression (OLR) model to predict the probabilities of LVP categories at Vienna International Airport. Lei et al. (2017) have used standard and hourly weather observations at Urumqi International Airport in China to develop a regression-based visibility prediction model using Deep Learning. Bari (2018) has assessed the potential of two machine-learning techniques (XGBoost and Deep Learning) to predict horizontal visibility based on the operational AROME-Morocco model outputs. The algorithms have been developed under the H2O³ open source platform. However, the performance of developed models differs from one study to another due to the variety of datamining tools and algorithms used.

Therefore, the objective of this study is to evaluate the sensitivity of the developed models performance to datamining platform and algorithm for a regression case, which aims to estimate the visibility from the operational numerical weather prediction AROME-Morocco model outputs.

2 Data and Methods

Corresponding to the raising importance of data mining, the number of available data mining tools continues to grow. Consequently, competition between data mining software developer's increases as well and the choice of the most suitable tool becomes increasingly difficult. Therefore, comparison of data mining tools becomes important. In this study, several, frequently used open-source data mining tools with open-source algorithms implementations are selected and compared against user groups, data structures, algorithms included, visualization capabilities, programming languages, and import and export options (Chen et al., 2007).

¹ <https://www.cs.waikato.ac.nz/ml/weka/downloading.html>

² <https://cran.r-project.org/>

³ <http://docs.h2o.ai/h2o/>

To achieve the aim of this study, we used two types of algorithms: those based on the ensemble based methods including gradient boosting machine (Friedman, 2001 and 2002), eXtreme gradient boosting (Tianqi and Guestrin, 2016) and random forest (Breiman, 2001), and those based on neural network, deep learning (Lecun et al., 2015; Schmidhuber, 2015; Goodfellow et al., 2016). The algorithms are evaluated under various open source platforms (Scikit-learn⁴, H2O, WEKA, Tensorflow and Keras⁵). In addition, a database covering 3-year of hourly data, and resulting from pre-processing of raw outputs of AROME-Morocco and observed data, were used in this work. The sampling of these data in 70% for learning and 30% for testing was carried out by guaranteeing the representability of months, hours and various classes of visibilities (below 1km; between 1 and 5km; above 5km) for all the synoptic stations. The study domain covers the north part of Morocco.

3 Results

The development of machine-learning based models using the datamining algorithms has been performed using the default configuration, then in the next step; we tuned the hyper-parameters using Grid Search and Random Search techniques for each datamining algorithm under the various open source platforms. This allowed us to obtain the best model for each algorithm with the optimum hyper-parameters.

The results analysis for the various algorithms used under the various platforms, shows that the performance of the ensemble-based models is the best whatever the platform used except for Keras where only deep learning was used. Thus, Random Forest algorithm is found to be the best estimator of visibility after hyper-parameters tuning under WEKA and Scikit-learn platforms. However, Gradient Boosting Machine outperforms the other algorithms for H2O platform. Root mean square errors are similar for the various platforms. Therefore, mean squared errors are 1933 m, 1942 m and 1945 m respectively for Gradient Boosting Machine under H2O, Random Forest under Scikit-learn and WEKA. Similarly, mean absolute error values are 1189 m, 1221 m and 1222 m for the same algorithms and platforms (Cf. Tab. 1).

Table 1: Mean absolute error (m) of the best model per datamining algorithm, per platform

	Mean absolute Error (m) of the best models			
	Deep Learning	Random Forest	Gradient Boosting Machine	XGBoost
	1563	1221	1186	1272
	1552	1245	1189	1382
	1903	1222		
	1506			

⁴ <https://scikit-learn.org/>

⁵ <https://www.tensorflow.org/guide/keras>

During the next step, we integrated the optimum hyper-parameters obtained either by Grid search or by Random search for a given platform, in the same algorithm but for another platform. In fact, Optimising hyper-parameters constitutes one of the most trickiest part in building the machine learning models. The primary aim of hyper-parameter tuning is to find the sweet spot for the model's parameters so that a better performance is obtained. In Grid Search, we try every combination of a preset list of values of the hyper-parameters and evaluate the model for each combination. Random search is a technique where random combinations of the hyper-parameters are used to find the best solution for the built model. Thus, it is possible that the hyper-parameters found for a given platform are not included in the range adopted for another platform during the optimization phase. Thus, we note that the performance statistics of the regressor model based on Random Forest and Gradient Boosting Machine are similar. For eXtreme Gradient Boosting, we notice that the regressor performance has slightly degraded under H2O with a difference of 222 m for RMSE and 110 m for MAE. For Deep Learning, it was found that the platform affects the regressor performance for the same hyper-parameters.

The model analysis based on the variable importance of the input parameters allowed us to identify which ones are highly weighted when estimating visibility from AROME-Morocco forecasts. In fact, we measure the importance of a feature by calculating the increase in the model's prediction error after permuting the feature. A feature is "important" if shuffling its values increases the model error, because in this case the model relied on the feature for the prediction. As result, the geographical position coordinates (latitude, longitude and altitude) are found to be the most important features since we are treating a regression problem at spatial scale over a large domain. In the second rank, it is found that 2m temperature and relative humidity, and also surface pressure and radiation have the highest importance.

4 Conclusion

In the present study, several contemporary open-source data mining platforms and algorithms were compared. Data mining software developers are answering to users paramount needs, resulting in minor differences between platforms. Each platform offers many data mining tasks. Evaluation of a regression process showed that there are some differences between platforms when using different algorithms.

5 References

Driss Bari. Visibility prediction based on kilometric NWP model outputs using Machine Learning regression. In 2018 IEEE 14th International Conference on e-Science (e-Science), pages 278–278. IEEE, 2018.

Ivana Bartoková, Andreas Bott, Juraj Bartok, and Martin Gera. Fog prediction for road traffic safety in a coastal desert region: Improvement of nowcasting skills by the machine-learning approach. *Boundary-layer meteorology*, 157(3):501–516, 2015.

Driss Bari and Mohamed El Khlifi. LVP conditions at mohamed v airport, Morocco: local characteristics and prediction using neural networks. *International Journal of Basic and Applied Sciences*, 4(4):354, 2015.

Philipp Kneringer, Sebastian J. Dietz, Georg J. Mayr, and Achim Zeileis. Probabilistic nowcasting of low-visibility procedure states at vienna international airport during cold season. *Pure and Applied Geophysics*, 176(5): 2165–2177, 2018.

Lei Zhu, Guodong Zhu, Lei Han, and Nan Wang. The application of deep learning in airport visibility forecast. *Atmospheric and Climate Sciences*, 7(03): 314, 2017.

Leo Breiman. Random forests. *Machine learning*, 45(1): 5–32, 2001

Jerome H Friedman. Stochastic gradient boosting. *Computational statistics & data analysis*, 38(4): 367–378, 2002.

Jerome H Friedman. Greedy function approximation: a gradient boosting machine. *Annals of statistics*, pages 1189–1232, 2001.

Tianqi Chen and Carlos Guestrin. Xgboost : A scalable tree boosting system. In *Proceedings of the 22nd acm sigkdd international conference on knowledge discovery and data mining*, pages 785–794. ACM, 2016.

Lecun, Yann, Bengio, Yoshua, and Hinton, Geoffrey. Deep learning. *Nature*, 2015, vol. 521, no 7553, p. 436.

Goodfellow, Ian, Bengio, Yoshua, and Courville, Aaron. *Deep learning*. MIT press, 2016.

Schmidhuber, J. Deep learning in neural networks: An overview. *Neural networks*, 61, 85-117. 2015.

Chen X, Ye Y, Williams G, Xu X. A survey of open source data mining systems. *Lecture Notes in Computer Science* 2007, 4819:3–14. 2007.

Case study to assess the precipitation forecast by Moroccan ALADIN configurations

Zahra SAHLAOUI

Abstract

Several model configurations are used in Morocco for numerical weather prediction (NWP). The aim of this work is to verify the impact of resolution on the quality of models forecast, particularly the precipitation field. Three model configurations are tested; ALADIN (7.5km), ALARO (5 km) and AROME (2.5 km). A rainy event over the North-East of Morocco is studied. The impact on models performances is assessed through the comparison of precipitation forecasts with the adjusted quantitative precipitation estimate from weather radar. The results show that AROME gives the best quality precipitation forecast in term of both intensity and localisation.

1 Introduction

Precipitation forecast is from great interest to human safety and economic activities. Producing high quality precipitation forecast is the aim of many improvements in the field of numerical weather prediction. But there are still some cases of under-over estimation of precipitation challenging the models accuracy.

In the present work, the ability of the model to improve precipitation forecast and the add value of finer resolution will be tested through numerical experiments using three limited area models (LAM) configurations that are ALADIN (7.5km), ALARO (5 km) and AROME (2.5 km). A case study over the North-East of Morocco will be carried. The impact on models performances will be assessed through the comparison of precipitation forecasts with the adjusted quantitative precipitation estimate from radar data.

2 Case overview

During the 19th January 2018, a meteorological perturbation affected the North-East of Morocco (figure 1.a). The situation was characterised by a surface depression centred on the East of Morocco and by geopotential minimum associated to cold air (-25°C) at 500hPa (figure 1.b). This configuration produced a cyclonic circulation bringing instable and humid air from the Mediterranean Sea (figure 1.c). Moderate precipitations reaching 30mm in 24 hours occurs over the North-East regions in Morocco during this situation.

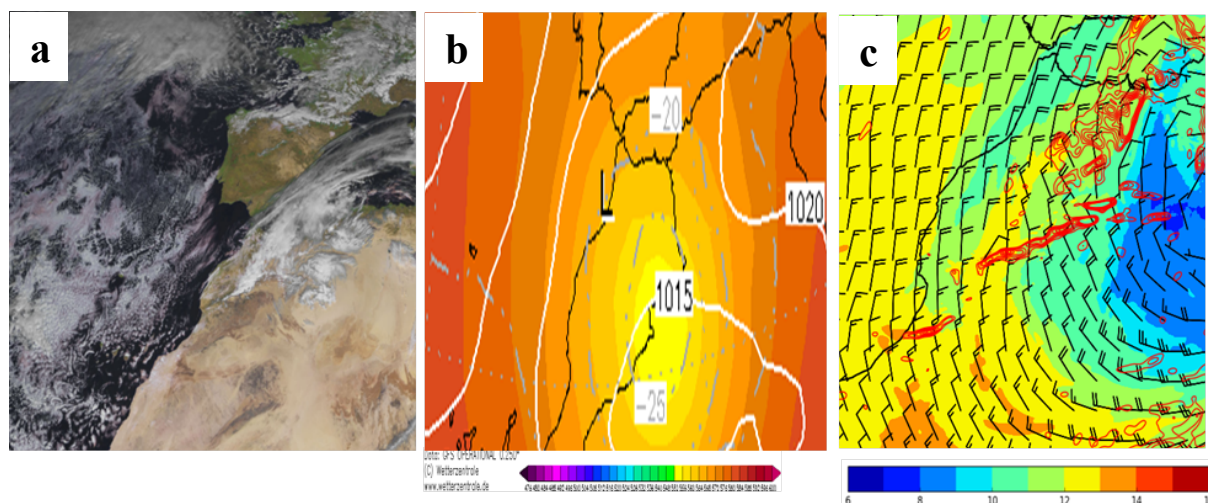


Figure 1: 19th January 2018 meteorological situation: a) MSG image at 12UTC, b) Surface pressure, geopotential and temperature at 500 hPa at 00UTC produced by GFS model, c) 600hPa wind, vertical velocity and temperature at 12UTC.

To evaluate the performance of each model, especially the accuracy of the precipitation forecast, three experiments were run. Indeed, The Moroccan Meteorological Service runs operationally three NWP models that are ALADIN, AROME and ALARO (table 1).

Model	Horizontal resolution	Dynamics
ALADIN	7.5 km	Hydrostatic
ALARO	5 km	Hydrostatic
AROME	2.5 km	Non-Hydrostatic

Table 1: characteristics of NWP models in Morocco

3 Forecast quality assessment

The forecast of cumulative precipitation amount was compared to the quantitative precipitation estimate produced by the Debdou radar and adjusted by the surrounding rain gauges [1].

Figure 2 shows the precipitation amount from the 19th at 06UTC to the 20th at 06UTC January 2018, produced by the three experiments and observed by Debdou radar. Two precipitations cells of more than 30mm are identified on the radar estimate (figure 2.a). The larger one (A) is located over Nador city and the surrounding area when the second one (B) is centred over Debdou city. The ALADIN experiment reproduces these two cells (figure 2.b) but the cell A is moved eastward. The ALARO experiment produces the same configuration as ALADIN with higher precipitation intensity for cell A and lower for cell B (figure 2.c). Concerning the AROME model, it produces the two cells with correct location and intensity (figure 2.d). Thus it can be deduced that this experiment is the best matching with the radar field.

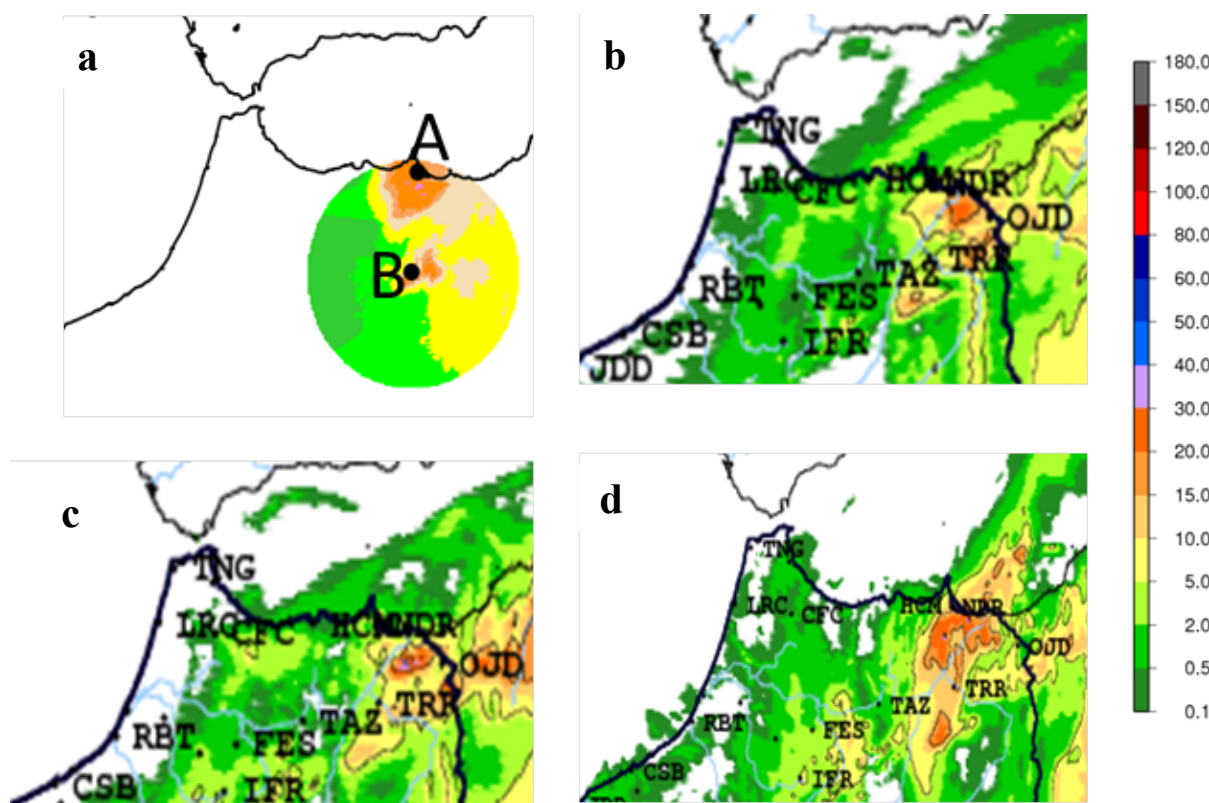


Figure 2: Precipitation amount from 19th at 06UTC to 20th at 06UTC January 2018, produced by Debdou radar (a), ALADIN (b), ALARO (c) and AROME (d).

4 Conclusion

This work was an opportunity to access the accuracy of precipitation forecast for many model resolution: ALADIN-7.5km versus ALARO-5km versus AROME-2.5km. Three experiments were run and the comparison with radar precipitation estimate allowed establishing relevant behaviour of each experiment. ALADIN and ALARO successfully reproduce the intensity of the main precipitation cells but the localisation was missed. The AROME model substantially improved the precipitation forecast for both intensity and localisation.

To have a global idea about each model configurations, more case studies should be carried over other regions and for both convective and stratiform precipitations. The use of SAL [2, 3] verification method will be required to bring out objective results.

5 References

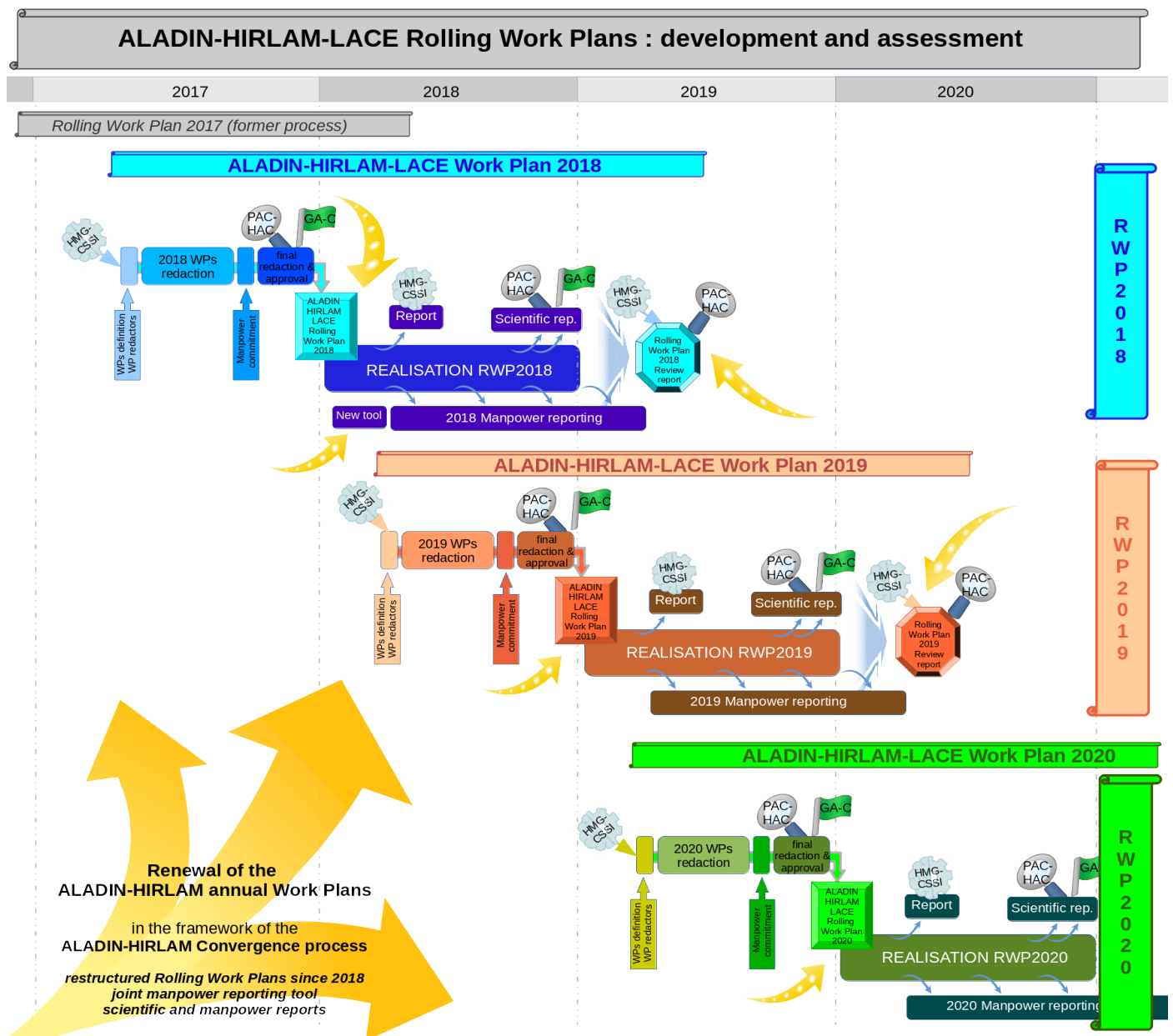
- 1 Z. Sahlaoui, S. Mordane, Radar Rainfall Estimation in Morocco: Quality Control and Gauge Adjustment. *Hydrology*, 6, 41, 2019.
- 2 H. Wernli, M. Paulat, M. Hagen, and C. Frei, SAL—A novel quality measure for the verification of quantitative precipitation forecasts, *Mon. Wea. Rev.*, 136, 4470–4487, 2008.
- 3 H. Wernli, H. Hofmann C, and M. Zimmer, Spatial Forecast Verification Methods Intercomparison Project: Application of the SAL Technique. *Wea. Forecasting*, 24, 1472–1484, 2009.

ALADIN-HIRLAM-LACE Rolling Work Plans development and assessment

Patricia Pottier

1 Introduction

According to [the ALADIN-HIRLAM cooperation agreement](#) signed in November 2016, the ALADIN Assembly and the HIRLAM Council shall annually decide upon the common research/work plan to be carried out. In the ALADIN-HIRLAM convergence process, the Directors tasked the PMs (1) to restructure this work plan identifying the various type of activities, (2) to report on its realisation and (3) to propose a manpower reporting tool to draw a global picture of manpower invested by the countries on the different activities of the work plan.



2 Re-structuration of the Work Plans

Development of the Rolling Work Plan 2018 (RWP2108) : April 2017 – November 2018

A major step was taken in April 2017 when the HMG-CSSI designed a seriously restructured work plan that makes the code contributions, the code engineering and the management of the codes more prominently visible. Technically, this work plan is organised in Work Packages, grouped in 3 sorts of activities (see Fig. 2); each Work Package is written under the responsibility of main editor(s); it contains a table of participants (and their effort in person.month, as committed by the ALADIN [LTMs](#) and the HIRLAM HoR), the objectives, the tasks and the deliverables (t-code and non-t-code). The PAC-HAC and the Directors approved this new structure.

The ALADIN/HIRLAM/LACE rolling work plan

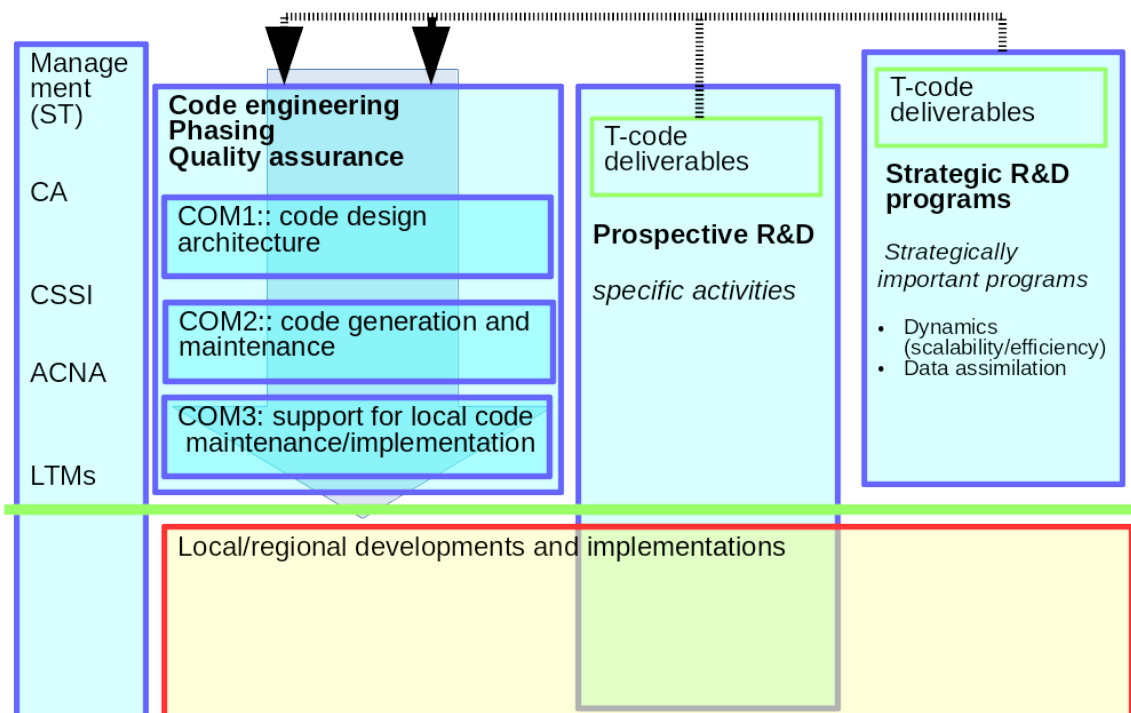


Fig 2: Structure of the Work Plan (version of Nov. 2018)
 “specific activities” : Work Packages for data assimilation, dynamics, physics parametrizations, surface analysis and modelling, ensemble forecasting and predictability, quality assurance and verification, technical code and system development, towards modelling at (sub-)km resolution



The first work plan written according to this new structure was [the common ALADIN-HIRLAM Rolling work plan for 2018](#), approved during the [3rd ALADIN GA & HIRLAM-C](#) in November 2017.

Realisation (2018) and progress assessment of the RWP2018 (April 2018 -May 2019)

[In April 2018, during their annual meeting](#), the HMG-CSSI reviewed the status of the 2018 Work Packages, most on their tasks being “on-track” at this early stage of their realisation period. They also agreed on a mechanism to jointly report about the progress of this plan within a year.

Early 2018, a **manpower reporting tool** had been developed. It was presented to the HMG-CSSI and demonstrated to the ALADIN LTMs and HIRLAM HoRs who have been using it quarterly since then (see Fig. 3). Some statistics (manpower by periods, by activities, by Work Packages, comparison between the manpower committed in the RWP and the manpower realised, ...) are produced on-line and available to each national representative (statistics over their national data) and to the Program Managers (statistics over their consortium).

FRANCE-LTM ACCOUNT, CORRESPONDANT FOR METEO FRANCE (FRANCE)
[Change my password](#)

MANAGEMENT OF METEO FRANCE PEOPLE ?
[Add a newcomer](#)
 Select a person to view and possibly update his/her data

CONSULT THE WORK ALREADY REPORTED ?
 Choose the person | 2019-04-01 | 2019-07-01 | [View reported work](#)

REGISTER 2019-04-01 - 2019-07-01 WORK

Who ? Choose the person | When ? 2019-04-01 | 2019-07-01 | Where ? FRANCE

Level of the funding of the work ? NMS level CONSORTIUM level

Choose the category of work ? | Link the work to the RWP | [Consult the 2019 RWP](#)

Subject : subject with, as far as possible, reference to the relevant task(s) in the selected WP | Weight ? : 1 0.5

Choose the duration of each type of work during the period ?

Total Duration ?	training ?	tuition ?	development ?	operational ?	maintenance ?	validation ?	management ?
0	0	0	0	0	0	0	0

[Register the action](#) [Reset the form](#)

SOME STATISTICS

[Last quarter \(2019-04-01 - 2019-07-01\)](#) [Previous quarter \(2019-01-01 - 2019-04-01\)](#) [Last year \(2018-07-01 - 2019-07-01\)](#)
[Annual and quarterly statistics](#)
[2018 commitments and realization](#) [2019 commitments and realization](#)

Fig 3: Screenshot of the manpower reporting tool (early 2019)

Throughout 2018, the PMs have reported on the scientific achievements and on the manpower dedicated to the RWP2018 (PAC-HAC, Directors). During the [4th joint ALADIN-GA & HIRLAM-C meeting](#) in November 2018, the PMs made these statistics concrete when presenting some important achievements among the Strategic and R&D Work Packages.

[Early 2019, the HMG-CSSI](#) reported on the status of each task in the RWP2018 Work Packages sheets. The ALADIN LTMs and the HIRLAM HoRs finalized their reporting on the manpower dedicated to the RWP2018 by their teams in 2018



During the HMG-CSSI meeting in April 2019, the document [“Status of the RWP2018”](#) was assessed and illustrated with some statistics of the committed vs declared manpower.

Global picture of the annual contributions by countries to the different activities of the RWP

The realisations (as reported in the manpower tool) over 2018 are higher than the commitments (in the RWP2018), probably due to (1) an underestimation of the commitments when committing for the first time the manpower in the newly structured RWP2018 and (2) more accurate manpower reporting with the use of the new reporting tool (see Fig.4).

Manpower (in F.T.E.) in 2018 & 2019 RWP Work Packages

Committed in RWP2018, Reported in manpower DB in 2018, Committed in RWP2019

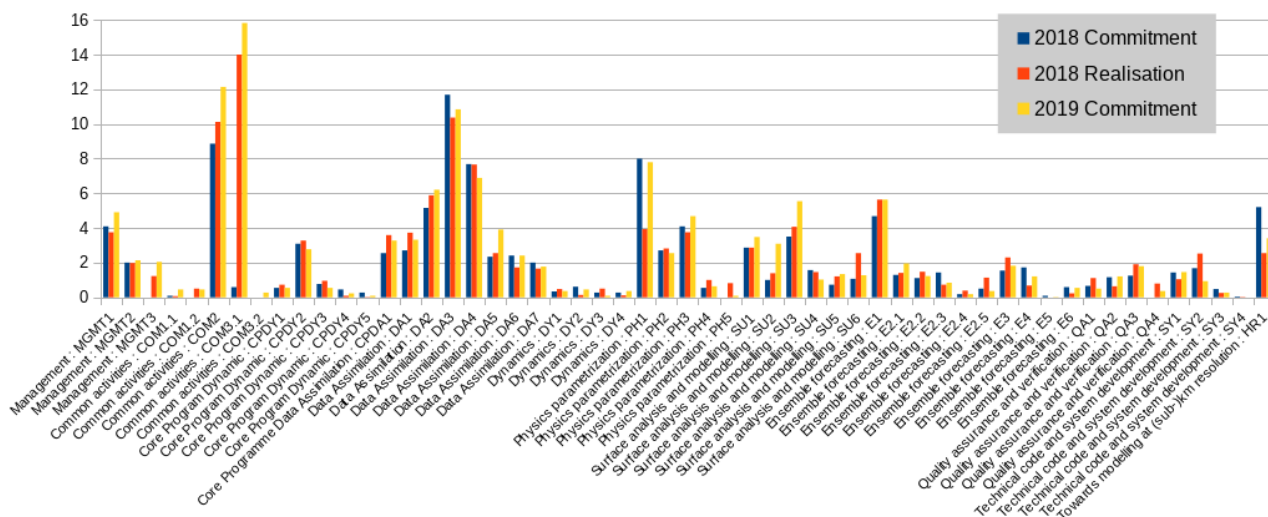


Fig 4 : Manpower (in Full Time Equivalent) committed to the Work Packages in RWP2018 (blue) and in 2019 (yellow), compared with the Manpower reported in 2018 (in orange)

The distribution of the manpower (either committed or reported, see Fig.5) by grouping of Partners (HIRLAM, LACE, Météo-France MF, FR i.e. ALADIN Partners besides LACE and MF) is very stable, around 1/4 for each grouping (23% for HIRLAM and LACE, a bit less for FR while MF take up the biggest contribution). Statistics by countries or by Work Packages have also been produced.

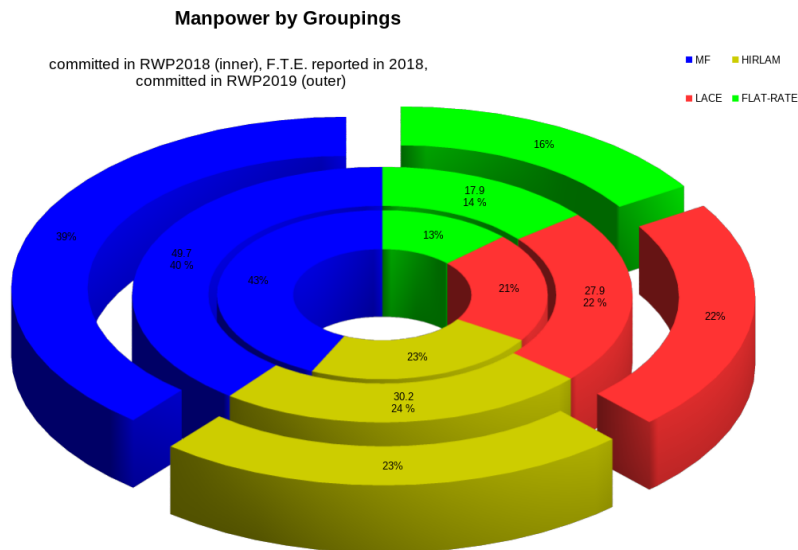


Fig 5 : Manpower committed in RWP2018 (inner circle) and in RWP2019 (outer circle) and realised in 2018 (central circle) by groupings of Partners (HIRLAM in yellow, LACE in red, MF in blue, FR in green)

Preparation for RWP2019 (April 2018 – November 2018)



In April 2018, the HMG-CSSI also worked on the main structure of the 2019 Rolling Work Plan : the list of the 2019 Work Packages was adapted from the 2018 list, together with their lead authors. The timeline for the preparation of the 2019 RWP was agreed, together with revisited editorial guidelines.

The main redaction period covered May to mid-September; the ALADIN LTMs and the HIRLAM HoR committed then the manpower in the different Work Packages and their tasks. Following PAC-HAC recommendations, the [4th joint ALADIN GA & HIRLAM C](#) approved [the RWP2019](#).

A Rolling story ...

[Last April, the HMG-CSSI](#) not only assessed the Status of the RWP2018, but quickly reviewed the first realisations of the RWP2019 and also prepared for the RWP2020 (adaption of the Work Packages list, main authors, writing guidelines, timeline,). The preparation of RWP2020 is going through the same steps as for RWP018 et RWP2019. Meanwhile the RWP2019 realisation is monitored and its progress reported.

Next steps ...



ALADIN and HIRLAM teams are realising the RWP2019, reporting on it and are preparing the RWP2020 (to be adopted at the 5th joint ALADIN-GA & HIRLAM-C in December 2019). The status report of the RWP2019 is due in Spring 2020 after the HMG-CSSI meeting.



3 To know more

The approved Rolling Work Plans and their summary status reports are published on [the ALADIN webpage dedicated to the Rolling Work Plans](#).

More details about the realisation of the Work Packages are available in the [minutes of the HMG-CSSI meetings](#) or can be asked to the HMG-CSSI members and/or the Work Packages editors.

They are also presented to PAC-HAC meetings and Directors Assemblies : see [the PAC-HAC minutes](#) or the [on-line presentations and minutes of the joint ALADIN-GA & HIRLAM-C meetings](#).

Besides the on-line graphics and statistics available to the PMs, LTMs and HoR through the manpower monitoring tool, the statistics produced for the HMG-CSSI, PAC-HAC and Directors meetings or additional on-demand statistics should be asked to Patricia.

Previous issues of the joint ALADIN-HIRLAM NL

No.12 January 2019



ALADIN-HIRLAM Newsletter
No. 12, January 31st, 2019



2018 Grand Tour of ALADIN & HIRLAM

ALADIN Programme, c/o P. Termonia, IRM, Avenue Circulaire 3, 1180 Bruxelles, Belgium
HIRLAM-C Programme, c/o J. Onvlee, KNMI, P.O. Box 201, 3730 AE De Bilt, The Netherlands

No.11 August 2018



No. 10. January 2018



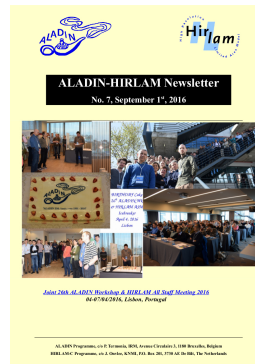
No. 9. September 2017



No. 8. January 2017.



No. 7. September 2016



No. 6. February 2016.



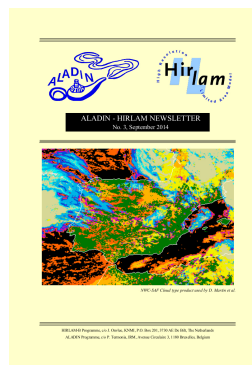
No. 5. August 2016



No. 4. February 2015



No. 3. September 2015



No. 2. April 2014



No. 1. September 2013

